TOPICAL REVIEW

Shapes and collectivity of exotic nuclei — The first decade of low-energy Coulomb excitation with radioactive ion beams

Andreas Görgen

CEA Saclay, IRFU/Service de Physique Nucléaire, F-91191 Gif-sur-Yvette, France

Department of Physics, University of Oslo, PO Box 1048 Blindern, N-0316 Oslo, Norway

Abstract. The way in which an atomic nucleus responds to excitations, whether by promoting individual nucleons into higher shells or by collective rotation or vibration, reveals many details of the underlying nuclear structure. The response of the nucleus is also closely related to its macroscopic shape. Low-energy Coulomb excitation provides a well-understood means of exciting atomic nuclei, allowing the measurement of static and dynamic electromagnetic moments as a probe of the nuclear wave functions. Due to the availability of radioactive heavy-ion beams with energies near the Coulomb barrier it is now possible to study the shape and collectivity of short-lived exotic nuclei, providing a particularly stringent test of modern theoretical nuclear structure models. This review gives an introduction to the experimental techniques related to low-energy Coulomb excitation with radioactive ion beams and summarizes the results that were obtained over the last ten years for exotic nuclei across the entire nuclear chart at various laboratories employing the isotope separation on-line technique.

PACS numbers: 21.10.Re, 23.20.Js, 25.70.De, 29.38.Gj

Submitted to: *J. Phys. G: Nucl. Phys.*

1. Introduction and overview

The shape is one of the most fundamental properties of an atomic nucleus, along with its mass and radius. It is governed by a delicate interplay of macroscopic, liquid-drop like properties of nuclear matter and microscopic shell effects. Collective rotations and vibrations are the dominant modes of excitation in deformed nuclei. The properties of collective excitations are very sensitive to the underlying nuclear shape and their experimental study contributes significantly to our understanding of the nuclear many-body problem. The motion of individual nucleons depends critically on the nuclear shape, and conversely the shape can be strongly influenced by a few individual nucleons. Systematic spectroscopic studies over more than 50 years have yielded a wealth of data that led to the development of microscopic descriptions of collective nuclei, for which the foundation was laid in the work of Bohr and Mottelson [1].

Today we have means to study collective excitations and shapes of exotic nuclei, *i.e.* short-lived nuclei far from stability. By measuring collective properties of exotic nuclei we can test the predictive power of theoretical models that were developed to describe nuclei close to stability. The population of specific neutron or proton orbitals in exotic nuclei can lead to unusual phenomena. These can for example be related to the occupation of the same proton and neutron orbitals in heavy $N = Z$ nuclei, or to the combination of weakly bound neutrons and deeply bound protons in neutron-rich nuclei. Additional motivation to study the collectivity of exotic nuclei is found in nuclear astrophysics, as spectroscopic properties of certain exotic nuclei are important for the understanding of nucleosynthesis in stars and cataclysmic stellar events.

The interest in the collectivity of exotic nuclei is not restricted to regions where deformed shapes are found. The measurement of collectivity in the proximity of closed shells gives insight into the evolution of the nuclear shell structure far from stability. It is by now well established that the usual magic numbers 8, 20, 28, 50, 82, and 126 are not universal. Structural changes in exotic nuclei can lead to a quenching or even complete disappearance of shell closures, whereas new magic numbers can emerge [2]. Much effort is for example devoted to studying the collectivity of nuclei in the vicinity of exotic ${}^{78}_{28}\mathrm{Ni}_{50}$, ${}^{100}_{50}\mathrm{Sn}_{50}$, or ${}^{132}_{50}\mathrm{Sn}_{82}$.

Large-scale shell model calculations are commonly used to describe the structure of exotic nuclei near shell closures (see [3, 4, 5] for reviews). Quadrupole deformation is described in the shell model as quadrupole excitations of the core coupled to the valence orbitals and is accounted for by introducing effective charges for the protons and neutrons. Experimental measurements of $E2$ transition strengths and quadrupole moments represent important benchmarks for such calculations. Shell model calculations, however, become intractable for heavy open-shell nuclei, for which the only viable theoretical descriptions are based on self-consistent mean field approaches. The latter have seen tremendous progress in recent years due to the introduction of correlations beyond the mean field (see *e.g.* the review of Bender, Heenen, and Reinhard [6]). Of particular relevance for the description of nuclear shapes and shape coexistence are extensions of the mean-field approach that allow configuration mixing, *i.e.* the superposition of several mean-field states, for example using the generator coordinate method (GCM). Such calculations have been performed using effective interactions of Skyrme (*e.g.* [7, 8, 9]), Gogny (*e.g.* [10, 11, 12]), and relativistic mean field (*e.g.* [13, 14]) type, and much effort is currently devoted to developing a non-empirical and universal formulation in the language of density functional theory. GCM

calculations provide both excitation spectra and electromagnetic matrix elements without introducing additional parameters beyond those of the underlying energy density functional, making the measurement of transition probabilities and quadrupole moments an important experimental tool to test the theoretical predictions, in particular for exotic nuclei.

The nuclear chart contains less than 300 stable nuclides along the so-called valley of β stability. About 3000 α- or β-unstable nuclides have been produced in laboratories, and more than 6000 nuclides are thought to be bound by the nuclear force, *i.e.* stable against proton or neutron emission. The science of exotic nuclei is a vast and very active field or research today [15, 16, 17]. Facilities producing radioactive ion beams (RIB) are at the core of the world-wide effort to study exotic nuclei. In general one distinguishes two types of facilities to produce energetic RIB: those that produce radioactive ions in flight and those using the isotope separation on-line (ISOL) technique. In-flight facilities use fragmentation, spallation, or fission of primary heavy-ion beams at intermediate or relativistic energies (50 MeV to 1.5 GeV per nucleon). The production targets are thin enough to allow the separation of the recoiling products in electromagnetic separators. ISOL facilities, on the other hand, use a driver accelerator to induce reactions in thick targets. The produced radioactive isotopes that diffuse out of the target are subsequently ionized and accelerated in a post-accelerator. In-flight facilities have the advantage that the production is independent of the chemistry of the desired element and fast, giving access to very short-lived nuclei. ISOL facilities are superior for experiments that require secondary RIB at well-defined energies at or below the Coulomb barrier. Complementary studies of nuclear collectivity are performed both at in-flight and ISOL facilities. Nuclear spectroscopy with fast exotic beams has recently been reviewed by Gade and Glasmacher [18]. The goal of the present article is to review studies of shapes and collectivity in exotic nuclei by low-energy Coulomb excitation with ISOL beams.

The measurement of dynamic and static electromagnetic moments represents one of the most sensitive probes of nuclear structure and the most direct method to study nuclear collectivity and shapes. Coulomb excitation selectively excites low-lying collective states with cross sections that are a direct measure of the electromagnetic matrix elements. At low energy the excitation process is dominated by the well-known electromagnetic interaction, while contributions from the nuclear force are insignificant. Low-energy Coulomb excitation therefore allows quantitative nuclear structure studies unimpeded by incomplete knowledge of the nuclear interaction and reaction mechanism. Coulomb excitation has been pioneered in the 1950's and was extensively used during the 1960's and 70's when heavy-ion accelerators and high-resolution germanium detectors became readily available. However, the technique was limited to stable or very long-lived nuclei. Low-energy Coulomb excitation of unstable nuclei became feasible only when ISOL-based RIB facilities became operational around the turn of the millennium. The technique of low-energy Coulomb excitation has since then seen a renaissance, with ambitious experimental programmes being pursued world-wide. It seems therefore timely to review the progress that has been made in this field over the last decade.

The article is organized as follows: The fundamental relations for electromagnetic transition probabilities and quadrupole moments, *i.e.* the observables characterizing nuclear collectivity and shapes, are summarized in section 2, followed by a discussion of the experimental techniques related to low-energy Coulomb excitation with RIB in section 3. The ISOL facilities where such experiments are routinely performed are

briefly described in section 4, and examples for studies of shapes and collectivity in exotic nuclei by low-energy Coulomb excitation are presented in section 5. For each case the physics context is briefly introduced, specific experimental aspects related to the use of RIB are mentioned, and the principal results and their impact on the field of nuclear structure is discussed. Since low-energy Coulomb excitation studies with RIB are now very actively pursued in several laboratories with many projects in progress, completeness for the selection of examples was not attempted. The last section 6 finally gives a summary and an outlook to future perspectives in particular in the light of the new RIB facilities which are under construction.

2. Electromagnetic transition probabilities and quadrupole moments

The goal of Coulomb excitation experiments is to extract information on the nuclear structure of excited states from electromagnetic matrix elements. The transition probability for an electromagnetic transition of multipolarity $\sigma\lambda$ (where σ denotes either electric or magnetic character and λ the angular momentum) between states of spin I_1 and I_2 is given by (see Bohr and Mottelson [1] for more details)

$$B(\sigma\lambda; I_1 \rightarrow I_2) = \sum_{\mu M_2} |\langle I_2 M_2 | \sigma\lambda\mu | I_1 M_1 \rangle|^2 \tag{1}$$

$$= \frac{1}{2I_1+1} |\langle I_2 || \sigma\lambda || I_1 \rangle|^2 \,, \tag{2}$$

where the summation over magnetic sub-states is performed using the Wigner-Eckart theorem. The reduced matrix elements $\langle I_2 || \sigma\lambda || I_1 \rangle$ are observables in Coulomb excitation experiments. The electric quadrupole interaction is by far the most important multipolarity for Coulomb excitation, and the $B(E2)$ values represent the most significant measure of nuclear collectivity. A compilation of $B(E2; 0_1^+ \rightarrow 2_1^+)$ values for even-even nuclei across the entire nuclear chart can be found in [19]. Magnetic multipole excitation is generally weak in low-energy Coulomb excitation, but magnetic multipole matrix elements may become important for the decay of states that were populated by electric multipole excitation. The decay rate for a transition of multipolarity $\sigma\lambda$ is given by

$$T(\sigma\lambda; I_1 \rightarrow I_2) = \frac{8\pi(\lambda+1)}{\lambda[(2\lambda+1)!!]^2} \frac{1}{\hbar} \left(\frac{E_\gamma}{\hbar c}\right)^{2\lambda+1} B(\sigma\lambda; I_1 \rightarrow I_2) \,, \tag{3}$$

from which one obtains for example for $M1$ and $E2$ transitions:

$$T(M1) = 1.76 \cdot 10^{13}\, E_\gamma^3\, B(M1) \,, \tag{4}$$

$$T(E2) = 1.22 \cdot 10^{9}\, E_\gamma^5\, B(E2) \,, \tag{5}$$

where E_γ is the transition energy in MeV, the $B(E2)$ value is in units of $e^2\mathrm{fm}^4$, $B(M1)$ in μ_N^2, and the decay rates T in s^{-1}. The lifetime τ of a state is the inverse of the sum of partial decay rates. Using the phase convention of Krane and Steffen [20] one obtains the mixing ratio δ of a mixed $E2/M1$ transition with $\Delta I = 1$ as:

$$\delta(E2/M1) = 8.35 \cdot 10^{-3}\, E_\gamma \frac{\langle I-1 || E2 || I \rangle}{\langle I-1 || M1 || I \rangle} \,, \tag{6}$$

with E_γ in MeV and the electric and magnetic matrix elements in $e\mathrm{fm}^2$ and μ_N, respectively.

While off-diagonal matrix elements characterize the transition from one state to another, diagonal matrix elements describe transitions between magnetic substates of the same state and are related to static moments. Again, the quadrupole multipolarity is of particular importance. The diagonal $E2$ matrix element is related to the spectroscopic electric quadrupole moment Q_s, which measures the quadrupole deformation of the charge distribution in the laboratory frame of reference for a given state I:

$$Q_s(I) = \sqrt{\frac{16\pi}{5}} \frac{\langle I\, I\, 2\, 0 \,|\, I\, I\rangle}{\sqrt{2I+1}} \langle I||E2||I\rangle \,, \tag{7}$$

where $\langle I\, I\, 2\, 0 \,|\, I\, I\rangle$ is a Clebsch-Gordan coefficient. In the rotational model Q_s can be transformed into the intrinsic quadrupole moment Q_0 for axially symmetric shapes via

$$Q_s(I) = \frac{3K^2 - I(I+1)}{(I+1)(2I+3)} Q_0 \,, \tag{8}$$

where K is the projection of the angular momentum I onto the symmetry axis of the nucleus. Note that K is not a good quantum number for nuclei without axial symmetry. The sign of the intrinsic quadrupole moment Q_0 is positive for prolate and negative for oblate shapes, respectively. One can see immediately that the spectroscopic quadrupole moment is zero for states with $I = 0$, and that spectroscopic and intrinsic quadrupole moments have opposite signs for states with $K = 0$ and $I \neq 0$. The perceived shape of a nucleus in the laboratory frame of reference is hence different from the intrinsic shape, and the measurement of the sign of the spectroscopic quadrupole moment does not yet give an unambiguous and model-independent indication of the intrinsic shape. To relate the $E2$ transition probability with the intrinsic nuclear shape, a transition quadrupole moment Q_0^t can be defined through the relation

$$B(E2; I_1 \rightarrow I_2) = \frac{5}{16\pi} Q_0^t \langle I_1\, K\, 2\, 0 \,|\, I_2\, K\rangle \,. \tag{9}$$

For purely rotational states within a rotational band it is assumed that neither K nor the intrinsic quadrupole moment Q_0 change, and in that case it is $Q_0^t = Q_0$. One should keep in mind that $B(E2)$ values and spectroscopic quadrupole moments are the only observables related to quadrupole collectivity and shape, and that intrinsic shape parameters are generally extracted in a model-dependent way. However, in the exceptional case where a complete set of transitional and diagonal $E2$ matrix elements connecting all low-lying states is known, intrinsic deformation parameters can be extracted model-independently by evaluating rotationally invariant products of the matrix elements [21]. A compilation of electric quadrupole moments can be found in [22].

3. Experimental techniques

This chapter describes experimental techniques for the measurement of electromagnetic transition rates and quadrupole moments in exotic nuclei with a focus on low-energy Coulomb excitation. The alternative methods of intermediate-energy Coulomb excitation and Doppler-shift lifetime measurements are briefly mentioned at the end of this section.

3.1. Low-energy Coulomb excitation

Coulomb excitation is the excitation of a nucleus in the electromagnetic field that acts between two nuclei in a scattering process. At energies well below the Coulomb barrier the distance of closest approach between projectile and target is sufficiently large for the short-range nuclear interaction to be negligible. In that case one speaks of low-energy or *safe* Coulomb excitation. The criterion

$$d > [1.25(A_p^{1/3} + A_t^{1/3}) + 5]\,\mathrm{fm} \tag{10}$$

for the distance of closest approach between projectile and target is often used to ensure purely electromagnetic excitation [21]. If the de Broglie wavelength of the projectile is small compared to the distance of closest approach, and if the energy absorbed in the excitation is small compared to the centre-of-mass energy, the Coulomb excitation process can be described semi-classically, *i.e.* by classical treatment of the relative motion of projectile and target with quantal treatment of the excitation process. These conditions are usually fulfilled in low-energy Coulomb excitation. The excitation cross section can be described entirely by the matrix elements of the electromagnetic multipole moments and can be calculated with high precision. The monopole-monopole interaction between projectile and target gives rise to Rutherford scattering. Excitation of the projectile or target nucleus is caused by monopole-multipole interactions, while multipole-multipole interactions are usually negligible. The latter has to be distinguished from excitation of both projectile and target by independent monopole-multipole interactions in the same experiment. A comprehensive discussion of the theory of Coulomb excitation can be found in the monograph of Alder and Winther [23]. Only some experimental aspects that are specific to Coulomb excitation with RIB and relevant for the discussion of the examples in section 5 are outlined in the following.

Coulomb excitation was first observed in 1953 using light ions as projectiles [24, 25]. In such cases the electromagnetic interaction is weak and the excitation process, which is limited to single-step excitations, can be described by first-order perturbation theory. A few years later, with the availability of heavy-ion beams such as ^{16}O, ^{20}Ne, ^{32}S, or ^{40}Ar, multi-step Coulomb excitation was observed for the first time [26, 27]. Especially when high-Z projectiles such as ^{208}Pb are used, many states are populated in multiple steps, and the excitation process depends on a large number of matrix elements. When many states are populated it becomes increasingly difficult to extract the excitation probabilities directly from the spectra of the scattered particles. Instead the matrix elements can be extracted by comparing the intensities of the de-excitation γ rays with Coulomb excitation calculations. However, the γ-ray spectra can become very complicated and the analysis of such experiments became only feasible by using germanium detectors capable of resolving many γ-ray transitions. Another important step was the development of coupled-channel Coulomb excitation computer codes such as the widely used Winther-de Boer code [28], which allows the calculation of excitation cross sections from a set of electromagnetic matrix elements. The inversion of the problem, *i.e.* the extraction of the matrix elements from the observed γ-ray yields, however, is not straight forward due to complicated non-linear dependencies. The code GOSIA has been developed to overcome this difficulty by combining semi-classical Coulomb excitation calculations with a least-squares fitting of the matrix elements [29]. By measuring the γ-ray yields for different scattering angles and for projectiles (or targets) with different atomic numbers, it is in principle possible to obtain a sufficient number of independent data points to extract all relevant

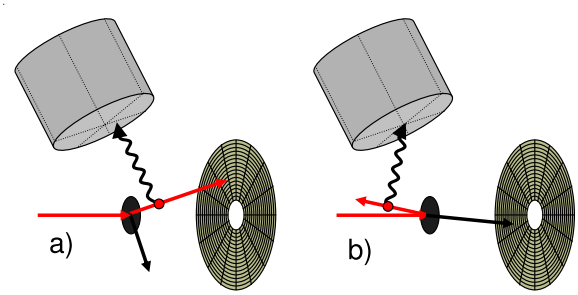

Figure 1. Schematic illustration of a typical Coulomb excitation setup. Either the scattered projectile (a) or recoiling target nucleus (b) is detected in an annular DSSD. In this way the scattering angle can be determined and a large range of centre-of-mass scattering angles is covered by a single DSSD. The γ-rays emitted from the excited projectile or target nuclei are detected in an array of germanium detectors, which ideally covers 4π of solid angle.

matrix elements, since the Coulomb excitation cross sections depend strongly on these parameters. Using this technique it has been possible in several cases to extract very large and more or less complete sets of matrix elements connecting low-lying collective states (see *e.g.* [30, 31, 32, 33, 34]). Deformation parameters in the intrinsic frame of the nucleus can be extracted from such sets of matrix elements in a model-independent way using the method of rotational invariants [21]. The code GOSIA is also widely used today to analyze Coulomb excitation experiments with RIB.

While stable nuclei can be studied using either projectile or target Coulomb excitation, projectile excitation is the only option for studies of short-lived radioactive nuclei. The main challenge in experiments with RIB is the beam intensity, which is typically several orders of magnitude lower than in stable-beam experiments. It is therefore crucial that both particle and γ-ray detectors have high efficiency and cover a large solid angle. The setups used for Coulomb excitation experiments at the different ISOL facilities are rather similar: Typically an annular double-sided silicon detector (DSSD) is used a few centimeters downstream from the target to detect the scattered projectiles and recoiling target nuclei (see figure 1). If projectile and target nuclei are not too similar in mass, they can be identified by the energy deposited in the DSSD, and the kinematics of the scattering process can be fully reconstructed. In this way it is sufficient to place a single DSSD under forward angles to cover a large range of centre-of-mass scattering angles. In a differential Coulomb excitation measurement, *i.e.* the measurement of γ-ray yields as a function of scattering angle, a compromise has to be found between a large number of data points for separate ranges of scattering angles and a minimum level of statistic for each individual range. Due to the weak beam intensities, differential measurements with RIB have been achieved only in favorable cases. Separate measurements with different target materials to utilize the Z dependence of the excitation cross section are also rarely performed because of the significant amount of beam time they require.

Most Coulomb excitation experiments with RIB use compact arrays of segmented germanium detectors to detect γ rays. Depending on the half lives of the nuclei in the beam, background related to their radioactive decay can be severe. By recording coincidences with scattered projectiles or recoiling target nuclei detected

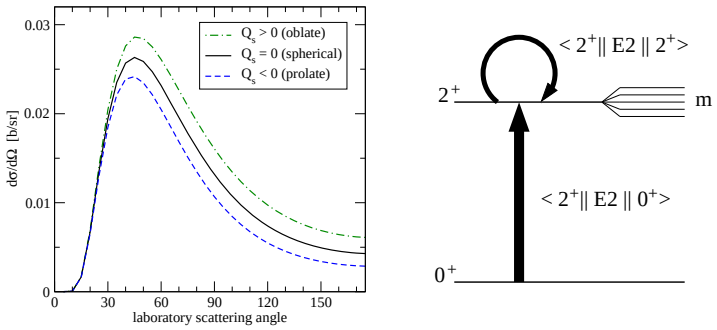

Figure 2. Calculated differential Coulomb excitation cross section to populate the 2_1^+ state for the example of ^{46}Ar scattered on ^{208}Pb. The three calculations assume the same transitional $\langle 2^+||E2||0^+\rangle$ matrix element, but different diagonal $\langle 2^+||E2||2^+\rangle$ matrix elements corresponding to oblate, spherical, and prolate shapes, respectively. The excitation process and the role of the reorientation effect are schematically illustrated on the right.

in the particle detectors, however, γ-ray background from the radioactive decay can be largely suppressed. Since γ rays from Coulomb excited states are emitted at high velocities of typically $v \approx 0.1c$, it is important to determine the angle between the γ ray and the velocity vector of the scattered particle to correct for the Doppler shift. The use of segmented germanium detectors with position sensitivity leads to a high spectral quality with reduced Doppler broadening even in a compact geometry with high efficiency. In experiments where both the projectile and target nucleus are excited, a Doppler correction has to be performed separately for the two velocity vectors. Due to the alignment of the nuclear spins in the scattering process, the emitted γ rays have an anisotropic angular distribution. The geometry and relative efficiency of the detectors has to be taken into account to compare the measured γ-ray intensities with Coulomb excitation calculations. To calculate γ-ray yields from the matrix elements one has to integrate over the angular ranges of scattered particles and γ rays, and also over the energy range of the projectiles which are slowed when traversing the target.

For experiments aiming at multi-step projectile excitation it is advantageous to use a ^{208}Pb target. The excitation probability for the target is then negligible due to the doubly magic character of ^{208}Pb, which simplifies the analysis. On the other hand the cross section for projectile excitation is large due to the high Z of the target. When the excitation probability is large, second-order effects become important, which can contribute additional information on the electromagnetic matrix elements. A second-order excitation can be understood as the virtual excitation of an intermediate state, which can lie either below or above the final state, and which can also be a magnetic sub-state of the final state. The influence of second-order transitions between magnetic sub-states is referred to as the *reorientation effect* [35]. Due to this effect the excitation probability depends also on the diagonal matrix element $\langle I||E2||I\rangle$, which is related to the spectroscopic quadrupole moment, and the Coulomb excitation process becomes sensitive to the nuclear shape. While the probability for first-order excitations is proportional to the square of the transitional matrix elements, interference terms in the second-order excitation process give sensitivity also to the sign of the matrix

elements. This dependence is illustrated in figure 2, which shows an example for the influence of the diagonal matrix element and its sign on the differential excitation cross section. The low intensities of RIB make reorientation measurements particularly challenging. Such experiments benefit considerably from an independent measurement of the lifetime of the state of interest, which depends only on transitional, but not on diagonal matrix elements. In addition to lifetimes of excited states experimental values for the branching and mixing ratios of decay transitions from complementary measurements can also be used as constraints in the analysis of Coulomb excitation experiments.

The spin alignment produced in the scattering process is attenuated by the hyperfine interaction with atomic electrons while the ions recoil from the target material into vacuum. The atomic electrons can produce very strong magnetic fields and electric field gradients, which interact with the magnetic dipole and the electric quadrupole moments, respectively. The resulting equilibration in the population of the magnetic sub-states (de-orientation) perturbs the angular distribution of the γ rays, which has to be taken into account in the data analysis. Generally neither the hyperfine fields nor the nuclear moments are known, so that models (*e.g.* [36]) have to be used. The de-orientation effect causes an additional systematic uncertainty in the measurement of electric quadrupole moments in Coulomb excitation experiments of typically a few percent, which is often negligible compared to the statistical uncertainty.

In many experiments with RIB only the excitation of the first excited state, *e.g.* the 2_1^+ state in an even-even nucleus, is observed due to the low level of statistics. Higher-lying states may be populated, but the cross section for their excitation is below the observational limit. In such cases only the transitional $\langle 2_1^+||E2||0_1^+\rangle$ matrix element can be extracted, although other matrix elements may contribute to the cross section, and their influence has to be considered to determine uncertainties. Sometimes rotational relations between matrix elements or values based on theoretical calculations are used in order to evaluate the coupling to higher-lying states and the influence of diagonal matrix elements. In experiments where only the integral excitation cross section to the first excited state was measured, it is convenient to choose a target material which is readily Coulomb excited by the projectiles and for which the matrix elements are well known. In this case the excitation probability of the projectile can be normalized to that of the target nucleus instead of using the Rutherford cross section for normalization. It is then not necessary to know absolute values for detector efficiencies, beam intensity, and target thickness. However, since RIB often suffer from isobaric contaminants, the exact beam composition has to be known and monitored to correct for target excitation by beam contaminants.

3.2. Intermediate-energy Coulomb excitation

Coulomb excitation at intermediate energies of typically 50 to 150 MeV per nucleon is an alternative technique to study the collectivity of exotic nuclei. While low-energy Coulomb excitation of exotic nuclei requires re-accelerated radioactive beams prepared with the ISOL technique, intermediate-energy Coulomb excitation is performed with fast fragmentation beams. Experiments to measure $B(E2)$ values in exotic nuclei using intermediate-energy Coulomb excitation have been performed since the 1990's at RIKEN [37], GANIL [38], NSCL / Michigan State University [39], and, at somewhat higher energies, at GSI [40]. The experimental technique has been

reviewed by Glasmacher [41], and the reader is referred to the review article on in-beam spectroscopy with fast exotic beams by Gade and Glasmacher [18] for more recent results. Although the discussion of results from intermediate-energy Coulomb excitation lies outside the scope of the present article, the principal differences between Coulomb excitation at low and intermediate energy shall be briefly discussed in the following.

It is an advantage of the in-flight production technique of RIB that it is independent of any chemical properties, which can impede the release of certain chemical elements from ISOL production targets. In-flight production is furthermore very fast, so that the lifetime of the nuclide to be studied is only limited by the flight time through the spectrometer which separates the nuclides of interest from other reaction products. A clean separation, however, is often difficult, resulting in secondary beams which contain only a small fraction of the nuclide of interest. An event-by-event identification of the ions before the secondary target is therefore usually necessary. Low beam intensities can be partly compensated by using relatively thick secondary targets, typically of several hundred mg/cm^2 thickness, so that it is usually possible to investigate nuclei further away from stability compared to low-energy Coulomb excitation.

In intermediate-energy Coulomb excitation experiments the contribution of the nuclear force and nuclear-Coulomb interference has to be excluded by selecting peripheral collisions corresponding to small scattering angles, so that the impact parameter exceeds the sum of the radii of projectile and target by several femtometer. Multi-step excitations are strongly suppressed due to high velocities and short interaction times, limiting the technique to states that can be reached in single steps. Since the influence of diagonal matrix elements is negligible for intermediate-energy Coulomb excitation, the technique is not sensitive to quadrupole moments, and usually it is applied only to determine the $B(E2; 0_1^+ \rightarrow 2_1^+)$ value in even-even nuclei.

Also for intermediate-energy Coulomb excitation the $B(E2)$ values are extracted by comparing experimental γ-ray yields with calculations of the Coulomb excitation cross sections. In the case of relativistic energies and large impact parameters the projectile trajectory can be approximated by a straight line. At intermediate energy relativistic retardation effects have to be considered, and the straight-line approach is no longer valid. Winther and Alder have given a semi-classical description of the process with a recoil correction that is achieved by rescaling the impact parameter [42]. The comparison with experimental results obtained using other techniques shows that intermediate-energy Coulomb excitation is a reliable approach to determine $B(E2; 0_1^+ \rightarrow 2_1^+)$ values in exotic nuclei with good precision [43].

3.3. Doppler-shift lifetime measurements

Electromagnetic transition probabilities can also be obtained by measuring the lifetime of excited states. Most low-lying states that decay by γ-ray emission have lifetimes in the range between 1 ps and 1 ns. The *recoil-distance Doppler shift* (RDDS) method is a well-established and well-adapted technique to measure lifetimes of excited states in this range. It utilizes the Doppler shift of γ rays emitted from excited nuclei recoiling out of a thin target foil with high velocity after heavy-ion induced reactions. A second foil, which is thick enough to stop the recoils, is mounted at a variable distance of some micrometers behind the target. Short-lived excited states decay while the recoiling nucleus is in flight between the two foils; longer-lived states decay only after the

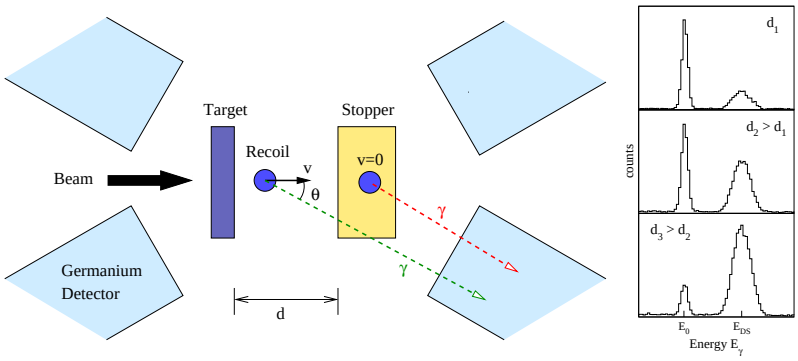

Figure 3. Schematic view of a plunger device surrounded by an array of germanium detectors. Typical γ-ray spectra, as seen in a detector under forward angle, are shown on the right-hand side for different plunger distances. The γ rays emitted from the stopper foil at rest appear at the transition energy E_0, while γ rays emitted in flight are Doppler shifted to higher energies. The flight peak is broadened mostly due to the finite opening angle of the germanium detector and velocity spread of the recoils.

recoils were stopped in the second foil. If the distance between the target and the stopper is such that the flight time of the recoil is of the same order as the lifetime of the state of interest, the γ-ray transition depopulating the state is observed with two components, shifted and unshifted, in a germanium detector mounted at either forward or backward angle with respect to the recoil direction. The lifetime of the state can then be extracted from the variation of the intensity ratio of the two components when changing the distance between the foils. The experimental setup of a RDDS measurement is illustrated schematically in figure 3. The apparatus which is used to adjust and control the distance between the two foils is commonly referred to as a *plunger*.

The RDDS method reaches its limit when the lifetime becomes comparable to the stopping time, which is typically of the order of $\sim$1 ps. When γ rays are emitted during deceleration of the recoils, their energy lies between that of the fully Doppler shifted and the stopped case, resulting in a characteristic line shapes in the γ-ray spectrum. Lifetimes in the range between $\sim$10 fs to $\sim$1 ps can be extracted from the Doppler-broadened line shapes using the so-called *Doppler shift attenuation* (DSA) method by comparing line shapes with simulations of the stopping process. More detailed descriptions of both the RDDS and DSA methods can be found *e.g.* in [44, 45].

In Doppler shift lifetime measurements the states of interest are usually fed from above, *e.g.* in fusion-evaporation reactions with heavy-ion beams. In order to extract the lifetime of a specific state one has to take into account the lifetimes and intensities of states and transitions feeding the state of interest. The fact that the precise feeding history is usually not known can cause large systematic errors. The problem of unknown feeding can be avoided by analyzing γ-γ coincidences, which allows selecting specific decay paths. The so-called *differential decay-curve method* [46] allows extracting the lifetime of a state from RDDS coincidence data independent of the lifetime of any feeding state. By requiring that a Doppler shifted component of a feeding transition was observed in coincidence with the decay of the state of interest, it is ensured that the recoiling nucleus was still in flight when the state was populated.

Under this condition the lifetime of the state can be determined from the intensities of the shifted and unshifted components of a depopulating transition alone without influence from feeding states.

Experiments using the RDDS technique after fusion-evaporation reactions have yielded electromagnetic transition probabilities for a wide range of nuclei throughout the nuclear chart. However, fusion-evaporation reactions with stable beams and targets can only populate neutron-deficient nuclei. Neutron-rich nuclei were inaccessible for RDDS measurements in the past, and so were nuclei which can only be produced in weak reaction channels for which the selectivity of the γ-ray spectrometers was insufficient to discriminate transitions from a large background. New techniques have been developed during the last few years which made the RDDS technique applicable also to very neutron-deficient and to moderately neutron-rich nuclei. The selectivity to measure lifetimes in nuclei populated in fusion-evaporation reactions with small cross sections has been improved by coupling a plunger device to a recoil mass spectrometer [47] or to a gas-filled recoil separator [48]. To allow the detection of fusion-evaporation residues in a spectrometer, the stopper foil of the plunger has to be replaced by a thinner foil, which only slows the velocity of the recoils without stopping them. The thickness of the degrader is chosen carefully to achieve a discernible difference in the Doppler shift of the transitions emitted before and after the degrader without impairing the performance of the spectrometer. The selectivity has been further increased by combining RDDS lifetime measurements with the *recoil decay tagging* technique, in which the prompt γ rays observed at the target position are correlated with a characteristic α decay [49, 50] or isomer decay [51, 52] observed at the focal plane of the recoil separator.

The RDDS technique has also been adapted to measure lifetimes of states in exotic nuclei populated in reactions induced by fast fragmentation beams. Both knock-out reactions [53] and intermediate-energy Coulomb excitation [54, 55] have been used to populate excited states in exotic nuclei. Moderately neutron-rich nuclei can also be produced in binary multi-nucleon transfer reactions, and RDDS lifetime measurements have been performed both for projectile-like [56] and target-like [57] reaction products by coupling a plunger device to a magnetic spectrometer. These new developments allow the measurement of transition strengths in exotic nuclei which have not been accessible before. Lifetime measurements are complementary to Coulomb excitation experiments and, as will be discussed in section 5, in some cases information on the nuclear shape could only be obtained from a combination of lifetime and Coulomb excitation measurements.

4. Isotope separation on-line facilities

The first isotope separation on-line experiment was performed as early as 1951 in Copenhagen by Kofoed-Hansen and Nielsen, who used a deuteron beam from a cyclotron to induce fission in uranium to study gaseous fission fragments after ionization and electromagnetic separation [58, 59]. The first major ISOL facility was installed by the ISOLDE collaboration at CERN in 1967. Today several ISOL facilities are operated world wide with the common principle of a driver accelerator to produce radioactive nuclides and an ion source coupled to the production target followed by a mass separator. The next extension of the technique was the introduction of post-accelerators to provide energetic beams of radioactive ions. With energies of typically 1 to 10 MeV per nucleon, secondary reactions can be induced by the

radioactive beams. The first facility of this type was operated in Louvain-la-Neuve [60, 61]. Low-energy Coulomb excitation experiments with radioactive projectiles require heavy-ion beams in the energy range between 2 and 5 MeV per nucleon produced by the ISOL method, and efficient detector setups for γ rays and scattered ions. This section briefly describes the four ISOL facilities with post-accelerators in which low-energy Coulomb excitation experiments are routinely performed today: ISOLDE at CERN, the Holifield Radioactive Ion Beam Facility (HRIBF) at Oak Ridge National Laboratory, the *Système de Production d'Ions Radioactifs Accélérés en Ligne* (SPIRAL) at GANIL, and the Isotope Separator and Accelerator (ISAC) at TRIUMF.

4.1. ISOLDE at CERN

At ISOLDE the radioactive nuclides are produced by proton-induced fission, spallation, or fragmentation reactions in thick, high-temperature targets of various materials. The proton beam is provided by the PS Booster accelerator with an energy of 1.4 GeV and a typical intensity of 2 μA. In some cases it is advantageous to use a neutron converter, *i.e.* to produce a flux of neutrons by proton-induced spallation reactions in a heavy metal target, which then induces fission reactions in a secondary uranium carbide target. The radioactive nuclides released from the target are ionized depending on their chemical properties either in a surface, plasma, or laser ion source. Resonant laser ionization is an efficient and selective method to ionize many metals and is often crucial for the production of secondary beams with high purity [62, 63]. Various options exist for the choice of the material and temperature of the transfer line between the target and ion source, which can be crucial for the suppression of unwanted contaminants. The singly-charged ions are extracted from the target ion-source unit with a potential of 60 kV and mass selected in either the general purpose separator (GPS) or the high resolution separator (HRS). In more than 40 years of operation ISOLDE has produced low-energy ion beams of more than 600 isotopes of more than 60 chemical elements. In principle all low-energy beams are available for re-acceleration in the REX post-accelerator [64], which started operation in 2001. The radioactive ions arriving continuously from either the GPS or HRS are first accumulated, bunched, and cooled in a Penning trap (REXTRAP) [65]. With a repetition rate of up to 50 Hz the singly-charged ions are released into the electron beam ion source REXEBIS [66] to breed a charge state with $A/q < 4.5$. After passing through an achromatic separator the highly-charged ions are injected into the room-temperature REX linear accelerator which can reach a maximum final energy of 3.0 MeV per nucleon.

The γ rays emitted after reactions of the radioactive beam on a secondary target are detected with the MINIBALL Ge detector array [67]. The array consists of eight modules with three encapsulated Ge detectors each. The detectors have a six-fold longitudinal segmentation resulting in a high granularity. Digital signal processing is used to determine the location of the first interaction of a γ ray. This position sensitivity allows operating the detectors at close distance from the target without loss of spectral quality due to Doppler broadening, resulting at the same time in a high efficiency. The MINIBALL array is coupled to a highly segmented annular double-sided silicon detector for the detection of scattered particles.

4.2. HRIBF at Oak Ridge National Laboratory

At the Holifield Radioactive Ion Beam Facility (HRIBF) [68] radioactive isotopes are produced in reactions between light ions from the Oak Ridge Isochronous Cyclotron and various target materials. Fission fragments are produced by 42 MeV protons impinging on a UC_2 target with intensities up to 10 μA. Other light-ion induced reactions such as (d,n), (p,2n), or (p,α) are used to produce radioactive isotopes *e.g.* in HfO_2 or liquid Ge targets [69]. The radioactive isotopes released from the target pass through a high-temperature transfer tube into a high-efficiency electron beam plasma ion source. The positive ions are extracted with a potential of typically 40 kV and pass through a mass analyzing magnet before entering a charge exchange cell. The latter is necessary to inject the beam into the 25 MV Tandem post-accelerator. Negative ions of halogen species can be directly produced in a negative-ion source. The target-ion source, the first-stage mass analyzer, and the charge exchange cell are located on a high-voltage platform, which is typically operated at 200 kV. The beam from the injector platform passes through a high-resolution isobar separator with a resolving power of $m/\Delta m \approx 20{,}000$ before acceleration in the Tandem. HRIBF delivered the first RIB in 1998, and the first RIB Coulomb excitation experiments were performed in 2001.

Coulomb excitation experiments at HRIBF are usually performed using the CLARION array [70] consisting of eleven segmented Clover and ten escape-suppressed coaxial germanium detectors. Each Clover detector consists of four individual crystals in a common cryostat, and each crystal is segmented into two halves. The detectors are placed at distances between 20 and 25 cm from the target and have a total photo-peak efficiency of approximately 2.6%. In some Coulomb excitation experiments where energy resolution was less crucial than efficiency, the CLARION array has been replaced by an array of BaF_2 detectors. In experiments which use a carbon target for the Coulomb excitation, recoiling carbon nuclei are detected in the HyBall array of CsI(Tl) charged-particle detectors. Experiments with heavier target materials use an annular segmented DSSD for the detection of both scattered projectiles and recoiling target nuclei.

4.3. SPIRAL at GANIL

The SPIRAL facility [71] at GANIL uses fragmentation of heavy ions to produce radioactive nuclides for post-acceleration. The heavy ions are accelerated subsequently in the two $K = 380$ cyclotrons CSS1 and CSS2 to energies up to 95 MeV per nucleon and impinge on a thick carbon production target. Typical beam intensities range from 2.5 pμA of ^{13}C for the production of neutron-rich He isotopes to 150 pnA of ^{78}Kr to produce neutron-deficient Kr isotopes. The production target is operated at high temperature of $\sim$2300 K to facilitate the migration of the reaction products to the surface. The radioactive atoms diffuse into a permanent magnet ECR ion source via a cold transfer tube, which largely prevents non-gaseous elements to reach the plasma of the source. The facility is presently limited to the production of isotopes of gaseous elements (He, N, O, F, Ne, Ar, Kr). The ECR source provides highly-charged ions which are extracted with a potential of $\sim$30 kV and which pass through a low-resolution separator with $m/\Delta m = 250$. The ions are then injected into the $K = 265$ CIME cyclotron, which accelerates the beams to energies ranging from 1.7 to 25 MeV per nucleon. The cyclotron itself provides a mass resolution of $m/\Delta m \approx 2000$. By

detuning the isochronism the mass resolution can be improved up to $m/\Delta m \approx 10{,}000$. SPIRAL is producing RIB since 2001.

The γ rays following Coulomb excitation are detected in the EXOGAM array [72] of up to 16 large segmented germanium Clover detectors. Each detector consists of four large germanium crystals and each crystal is longitudinally segmented into four sectors. The detectors can be placed either at 11.5 or at 14 cm distance from the target. In the compact geometry the detectors are only partly shielded against Compton-escape events, whereas in the distant configuration the germanium crystals are fully shielded by bismuth germanate (BGO) detectors. At the closer distance each Clover detector has a photo-peak efficiency of approximately 1%. The Coulomb excitation setup at SPIRAL uses a highly segmented annular DSSD detector for the detection of scattered particles, which is typically placed 25 mm downstream from the target.

4.4. ISAC at TRIUMF

The Isotope Separator and Accelerator (ISAC) [73] at TRIUMF uses the 500 MeV proton beam of up to 100 μA intensity from the TRIUMF cyclotron to produce radioactive nuclides in either metal (Ta, Nb) or carbide (SiC, TiC, ZrC) production targets. Various types of ion sources are available, including hot surface ion sources, mostly for the production of beams of alkali elements, a resonant laser ion source, and FEBIAD and ECR plasma ion sources. The ions are extracted by a high-voltage potential and pass subsequently through a mass separator. In a first stage, ISAC-I, the radioactive ions are accelerated in a radio-frequency quadrupole (RFQ) and room temperature linear accelerator to a maximum energy of 1.8 MeV per nucleon. The RFQ accepts ions with $A/q \leq 30$. Beams with $A > 30$ require higher charge states, which are produced in an ECR charge state booster. The beam from ISAC-I can be injected into the superconducting linear accelerator ISAC-II to increase the beam energy to a range between 5 and 11 MeV per nucleon. The first radioactive beams from ISAC-I and ISAC-II were delivered in 2001 and 2007, respectively.

Coulomb excitation experiments use the TIGRESS γ-ray spectrometer [74] and an annular DSSD for the detection of scattered ions. TIGRESS comprises 12 large segmented germanium clover detectors equipped with digital pulse processing electronics. Each Clover consists of four individual crystals. The outer contacts of each crystal are divided into eight segments, providing position sensitivity for the γ-ray detection.

5. Shapes and collectivity of exotic nuclei

In the following low-energy Coulomb excitation experiments are discussed which were performed at the four ISOL facilities described in the previous section. The common goal of these experiments was to study shapes and collectivity of exotic nuclei, but each case has its own more specific motivation, which will be discussed briefly. Each experiment with RIB has also its own experimental challenges, for which solutions must be found individually from case to case. The principal results of each experiment are discussed in the context of the specific physics case. Experiments addressing nuclei in the same region of the nuclear chart are grouped together. Completeness for the selection of examples was not attempted.

5.1. The neutron-deficient Na isotopes

The nuclear structure of neutron-deficient Na isotopes is of interest for the understanding of break-out reactions from the hot carbon-nitrogen-oxygen (CNO) cycles into the rapid proton capture process, which occur in the accretion layers of neutron stars in binary star systems. Depending on the temperature and pressure conditions, the break-out is thought to involve the reactions ^{18}Ne(α,p)^{21}Na and ^{15}O(α,γ)^{19}Ne(p,γ)^{20}Na [75]. Since resonant levels in these reactions are difficult to study experimentally in the laboratory, the understanding of these processes and of the reaction rates relies to a large extend on nuclear structure calculations. Although Coulomb excitation experiments do not give direct information relevant for the astrophysical processes, the measurement of transition matrix elements between low-lying states in these exotic nuclei is important as a sensitive test of the validity of the theoretical calculations.

Transition matrix elements in the neutron-deficient isotopes ^{20}Na [76] and ^{21}Na [77] were studied in the first Coulomb excitation experiments performed at the ISAC-I facility at TRIUMF. The radioactive isotopes were produced by proton-induced fragmentation of a Ta production target and subsequent ionization in a Re surface ion source. The radioactive ions were mass separated and accelerated to 1.7 MeV per nucleon in the ISAC-I accelerator. In the same experiment also the stable isotope ^{21}Ne was accelerated from an off-line source in order to measure matrix elements in the mirror pair ^{21}Na – ^{21}Ne. The projectiles were Coulomb excited on a natural Ti target, and γ-ray yields were measured for several ranges of scattering angles, which were determined from the detection of the projectiles or recoiling target nuclei in an annular DSSD detector. Transition matrix elements were determined relative to the well-known $B(E2;0^+ \rightarrow 2^+)$ value in the ^{48}Ti target nucleus using the code GOSIA. The experiments used an early implementation of the TIGRESS γ-ray spectrometer consisting at the time of two Clover detectors. The intensity of the radioactive beams was limited to $5 \cdot 10^6$ ions per second by the read-out capability of the detector electronics.

The first excited $5/2^+$ state in ^{21}Na was Coulomb excited from the $3/2^+$ ground state, and $B(E2;5/2^+ \rightarrow 3/2^+) = 136.5(92)$ e^2fm^4 was determined [77]. The lifetime of the $5/2^+$ state is known [78] and was used as additional input in the GOSIA calculation. With this constraint also the $M1$ transition strength could be determined to be $B(M1;5/2^+ \rightarrow 3/2^+) = 0.1513(17)$ μ_N^2 [77]. Prior to the Coulomb excitation experiment the $B(E2)$ value was only poorly known (48±41 e^2fm^4) due to the large uncertainty in the $E2/M1$ mixing ratio ($\delta = -0.05(2)$) [79]. With the direct measurement of the $B(E2)$ value by Coulomb excitation and the complementary lifetime information, the absolute value of the mixing ratio is now accurately determined to be $\delta = (+)0.0832(28)$. The attempt to extract its sign from the azimuthal yield distributions, however, remained inconclusive. The same analysis was performed for the stable ^{21}Ne projectile, and $B(E2;5/2^+ \rightarrow 3/2^+) = 87.5(58)$ e^2fm^4 was extracted, in agreement with the literature value of 83(10) e^2fm^4 [80]. Combined with the known lifetime [78], the mixing ratio and $B(M1;5/2^+ \rightarrow 3/2^+)$ value were also extracted for ^{21}Ne. The Coulomb excitation results show that the $B(E2)$ value is larger for ^{21}Na than for ^{21}Ne, contrary to previous results, which suggested the opposite. The new values for the $B(E2)$ and $B(M1)$ values are well reproduced by shell model calculations [77], so that the inconsistency related to the previous much smaller $B(E2)$ value for ^{21}Na could be resolved.

However, discrepancies between shell model calculations and experimental results were found in the Coulomb excitation experiment with ^{20}Na beam [76]. Excitation from the 2^+ ground state to the 3^+ and 4^+ first and second excited states was observed, and the GOSIA analysis yielded three matrix elements: $B(E2;3^+ \rightarrow 2^+) = 55.0(64)$ $e^2\mathrm{fm}^4$, $B(E2;4^+ \rightarrow 2^+) = 35.7(57)$ $e^2\mathrm{fm}^4$, and $B(M1;4^+ \rightarrow 3^+) = 0.154(30)$ μ_N^2. These results were compared with shell model calculations using the *sd* and $p-sd$ valence spaces with different effective interactions [76]. The $B(E2;4^+ \rightarrow 2^+)$ value was generally well reproduced, while the calculations systematically found too large $B(E2;3^+ \rightarrow 2^+)$ and too small $B(M1;4^+ \rightarrow 3^+)$ values. Since the calculations do not reproduce the transition strengths between the low-lying states satisfactorily, shell model predictions for higher-lying states should be taken with care. It is for example questionable if such calculations can be used to assign the spin-parity of the astrophysically important 2645 keV level [81]. The spin-parity assignment for this lowest level above the proton separation energy has a large impact on the rate of the ^{19}Ne(p,γ)^{20}Na reaction. With accurate results for transition strengths between low-lying states, Coulomb excitation experiments can help improving the theoretical description of exotic nuclei in this mass region.

5.2. The island of inversion around ^{32}Mg

The disappearance of a 'magic' shell gap in nuclei far from stability was first discovered in the so-called *island of inversion* around ^{32}Mg. Mass measurements for ^{31}Na and ^{32}Na were inconsistent with a spherical $N = 20$ shell closure and gave the first indication for a sudden onset of deformation [82]. The deformation was explained by the occupation of the neutron $f_{7/2}$ orbital in Hartree-Fock calculations [83]. Further evidence for the onset of deformation came from the observation of a low-lying 2^+ state in ^{32}Mg [84]. Shell model calculations restricted to the *sd* valence space could not explain the experimental results [85]. The discrepancies were explained by allowing neutron excitations from the $d_{3/2}$ to the $f_{7/2}$ orbital [86]. Systematic shell model calculations showed that for nuclei around ^{32}Na the deformed two-particle two-hole (*2p–2h*) configuration is energetically lower than the spherical closed-shell configuration [87].

The collectivity of nuclei within the island of inversion and at its borders has been extensively studied experimentally at fragmentation facilities using intermediate-energy Coulomb excitation and inelastic proton scattering. An overview over the experimental effort at intermediate energies can be found in [18]. The $B(E2)$ values for the neutron-rich Mg isotopes measured at RIKEN [37, 88], MSU [89, 90], and GANIL [91] are partly inconsistent and have been debated controversially. To clarify the situation low-energy Coulomb excitation experiments have been performed at ISOLDE with re-accelerated beams of neutron-rich Mg isotopes [92, 93]. Coulomb excitation of ^{30}Mg was the first spectroscopy experiment using the REX accelerator at ISOLDE and the MINIBALL Ge detector array. Details of this and subsequent low-energy Coulomb excitation experiments in this region are listed in table 1. The experiments used resonant laser ionization, resulting in rather pure radioactive beams with only little contamination from β-decay products of the short-lived isotopes (355 and 95 ms for ^{30}Mg and ^{32}Mg, respectively), which built up during trapping and charge breeding. The $B(E2;0_1^+ \rightarrow 2_1^+)$ values, which were obtained by normalizing the measured excitation probability of the projectile to that of the target nucleus, are shown in figure 4, where they are compared with results from intermediate-energy

Table 1. Experimental details and results from low-energy Coulomb excitation experiments for Na (TRIUMF) and Mg isotopes (ISOLDE).

Nuclide	Energy (A MeV)	Intensity (s^{-1})	Purity %	Target	$B(E2;\uparrow)$ (e^2fm^4)	Ref.
^{29}Na	2.41	600	72(1)	^{110}Pd	281(50)[a]	[108]
^{30}Mg	2.25, 2.69	10^5	82(1)	^{60}Ni, ^{107}Ag	253(21)	[92, 93]
^{32}Mg	2.84	$1.5 \cdot 10^4$	85(1)	^{107}Ag	434(52)	[93]

[a] $B(E2; 3/2^+_{g.s.} \rightarrow 5/2^+)$

measurements and theoretical calculations.

The $B(E2)$ values for ^{30}Mg and ^{32}Mg from the ISOLDE measurements are incompatible with the results from GANIL [91]. The value for ^{30}Mg supports the earlier result from MSU [89] and is well explained by shell model calculations within the *sd* valence space (*0p–0h* configuration), which suggests that ^{30}Mg lies outside the island of inversion. An excited 0^+_2 state based on the $\nu f^2_{7/2}$ configuration was recently identified by conversion electron spectroscopy of the electric monopole ($E0$) transition to the ground state [94], proving the coexistence of spherical and deformed shapes at the border of the island of inversion. For ^{32}Mg the results from RIKEN [37, 88], MSU [89, 90], and GANIL [91] scatter considerably. In the MSU experiments evidence was found for the population of an excited state in ^{32}Mg at 2321 keV excitation energy. The observed excitation cross section for the 2^+_1 state at 885 keV has consequently to be corrected for the feeding from the higher-lying state, which was hampered by its unknown spin and parity. A spin-parity of $J^\pi = 1^-, 1^+$ or 2^+ was assumed for the 2321 keV state, and two separate $B(E2)$ values with and without feeding correction were reported [89, 90]. Due to the relatively low beam energy used in the ISOLDE experiments, the measurement was only little influenced by real or virtual excitation of higher-lying states, and Coulomb-nuclear interference could be excluded. However, the excitation probability is influenced by the static quadrupole moment due to the reorientation effect. Motivated by theoretical predictions [10, 96] a prolate rotational model value for $Q_s(2^+_1)$ was assumed for both ^{30}Mg and ^{32}Mg in the analysis of the ISOLDE measurement. The resulting $B(E2)$ value is in good agreement with the results from RIKEN [37, 88] and those from MSU without feeding correction. Recent β-decay [97] and proton scattering experiments [98] confirm an earlier assignment of $J^\pi = 4^+$ for the 2321 keV state from in-beam γ spectroscopy [99]. The population of a 4^+ state by Coulomb excitation requires two-step excitation, which was not considered in the MSU intermediate-energy experiment.

The totality of the Coulomb excitation results, both at low and intermediate energies, confirm that ^{30}Mg is well explained by a spherical *0p–0h* configuration, whereas ^{32}Mg and ^{34}Mg have deformed *2p–2h* intruder configurations and lie within the *island of inversion*. Hyperfine-structure and β-NMR measurements have determined the magnetic moment and $J^\pi = 1/2^+$ for the ground state of ^{31}Mg [100], which provides evidence for an intruder configuration and strongly deformed ground state already in ^{31}Mg. A low-energy Coulomb excitation experiment with ^{31}Mg beam has been performed at ISOLDE recently [101], which is expected to help understanding the transition from normal to intruder configuration.

Anomalies related to the island of inversion were first discovered for the binding energies of ^{31}Na and ^{32}Na [82]. Large-scale Monte Carlo shell model (MCSM)

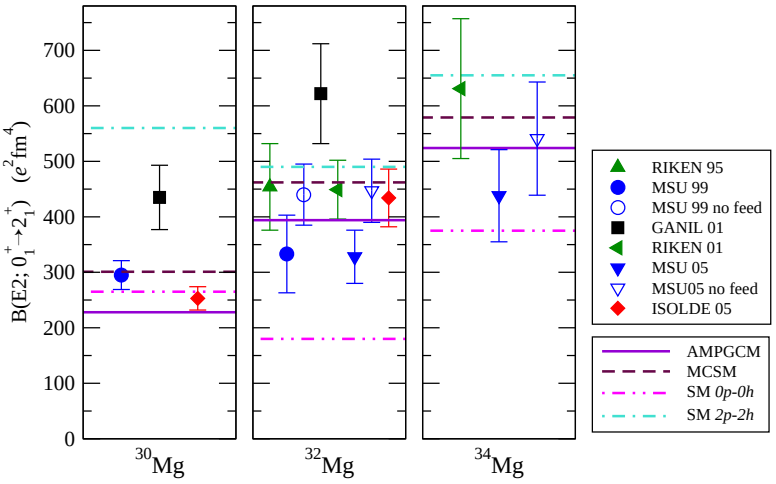

Figure 4. Comparison of experimental and theoretical $B(E2)$ values for ^{30}Mg, ^{32}Mg, and ^{34}Mg. Coulomb excitation experiments were performed at intermediate energy at RIKEN [37, 88], MSU [89, 90], and GANIL [91], and at low energy at ISOLDE [92, 93]. Separate results from the MSU experiments are shown with and without correction for feeding from higher-lying states (see text). The lines represent theoretical results from angular-momentum projected GCM calculations [10], quantum Monte Carlo shell model [95], and shell model calculations for normal and intruder configurations [96].

calculations using a valence space comprising the full *sd* shell and the two lowest *pf* shell orbitals find a rapid transition from a pure *0p–0h* configuration in the ground state of ^{27}Na and ^{28}Na via a strongly mixed configuration in ^{29}Na to a dominant *2p–2h* configuration in ^{30}Na and ^{31}Na [102]. Intermediate-energy Coulomb excitation has been performed for ^{28}Na [103], ^{30}Na [103, 104], and ^{31}Na [105]. The large $B(E2)$ value found for ^{31}Na is consistent with a deformed intruder ground state. The $B(E2; 2^+_{\text{g.s.}} \rightarrow 3^+)$ value measured for ^{30}Na is consistent with the MCSM calculations, but not with shell model calculations restricted to the *sd* shell only [102]. This comparison suggests that the intruder configuration is already dominant in the ground state of ^{30}Na. The level structure of ^{28}Na, ^{29}Na [106], and ^{30}Na [107] has been studied following β decay. The comparison of these results with shell model calculations show that intruder configurations become increasingly dominant with neutron number.

In order to better understand the transition from normal to intruder configurations for the chain of Na isotopes, a low-energy Coulomb excitation experiment has been performed with a ^{29}Na beam at the ISAC-II facility at TRIUMF [108]. Details of the experiment are included in table 1. Projectile excitation from the $3/2^+$ ground state to the low-lying $5/2^+$ state at 72 keV excitation energy was observed together with target excitation of the 2^+ state in ^{110}Pd, which was used for normalization. The γ-ray yields were analyzed using the code GOSIA. The quadrupole moment of the $3/2^+$ ground state is known experimentally [109] and was taken into account in the analysis. It was found that the $\langle 5/2^+||E2||5/2^+\rangle$ and $\langle 5/2^+||M1||3/2^+\rangle$ matrix elements and possible couplings to higher-lying states have only a small influence on the excitation probability, so that the $\langle 5/2^+||E2||3/2^+\rangle$ matrix element was the only free parameter. The resulting $B(E2)$ value is in good agreement with the MCSM calculations of Utsuno *et al* [102], further supporting the

interpretation of strongly mixed *0p–0h* and *2p–2h* configurations in ^{29}Na. Very recent Coulomb excitation measurements with ^{29}Na and ^{30}Na beams at ISOLDE are expected to provide more information on the transition from normal to intruder configurations at the border of the island of inversion.

5.3. Onset of collectivity near $N = 28$

While the $N = 20$ shell closure disappears abruptly between ^{34}Si and ^{32}Mg, the shell gap at $N = 28$ is reduced more gradually below ^{48}Ca. A small reduction of the shell gap for ^{46}Ar was deduced from neutron single-particle energies in ^{47}Ar [110, 111, 112]. For ^{44}S a collective 2_1^+ state [113] and the observation of a low-lying 0_2^+ state [114] suggests the presence of deformation and shape coexistence. The very low excitation energy of the 2_1^+ state in ^{42}Si [115] finally provides evidence for a substantial deformation and the collapse of the $N = 28$ shell closure.

Theoretical descriptions of the proton-deficient $N = 28$ isotones using the shell model [116, 117], the relativistic mean field approach [118], and the generator coordinate method (GCM) with Gogny interaction [117, 119] differ in some details, but result in a consistent overall picture, where the collectivity increases as protons are removed from ^{48}Ca. Both ^{46}Ar and ^{42}Si are predicted to have oblate shape, while ^{40}Mg is predicted to have large prolate deformation, and ^{44}S is found to be a good example for prolate-oblate shape coexistence. With nuclear shapes changing rapidly as a function of proton and neutron number, and with shape coexistence in some cases, electromagnetic transition rates and quadrupole moments are very sensitive to the changes in the underlying shell structure, and their measurement represents a stringent test of the different theoretical descriptions.

$B(E2; 0_1^+ \rightarrow 2_1^+)$ values in this mass region have been measured by intermediate-energy Coulomb excitation for ^{44}Ar [39], ^{46}Ar [39, 120], $^{38-42}$S [39], and ^{44}S [113]. Coulomb excitation at low energy, on the other hand, can also provide transition rates involving higher-lying states due to multiple-step excitation, and give information on spectroscopic quadrupole moments utilizing the reorientation effect. To test theoretical predictions for nuclear shapes in this mass region, a low-energy Coulomb excitation experiment [117] was performed using a ^{44}Ar beam from the SPIRAL facility at GANIL. The ^{44}Ar beam of $2 \cdot 10^5$ ions per second was produced by fragmentation of an intense primary beam of ^{48}Ca. To exploit the Z dependence of the excitation cross section, the ^{44}Ar projectiles were Coulomb excited on ^{109}Ag and ^{208}Pb targets at safe bombarding energies of 2.68 and 3.68 MeV per nucleon, respectively. The 2_1^+ and 2_2^+ states in ^{44}Ar were populated together with several states in the target nucleus ^{109}Ag, whereas target excitation for ^{208}Pb was negligible. The γ-ray yields were measured with EXOGAM for several ranges of scattering angles, which were determined using a segmented silicon detector. The excitation of the ^{109}Ag target nucleus was used for normalization purposes. Three transitional $E2$ matrix elements connecting the 0_1^+, 2_1^+, and 2_2^+ states and the diagonal matrix element for the 2_1^+ state were extracted from a fit of the γ-ray yields observed for various ranges of scattering angles and for the two different target materials using the code GOSIA. The $B(E2; 0_1^+ \rightarrow 2_1^+)$ value of 378^{+34}_{-55} e^2fm^4 [117] is in agreement with the value of 345(41) e^2fm^4 from intermediate-energy Coulomb excitation [39]. The spectroscopic quadrupole moment of the 2_1^+ state was found to be $Q_s(2_1^+) = -8(3)$ $e$fm^2 [117], indicating prolate deformation. In the rotational model the $B(E2; 0_1^+ \rightarrow 2_1^+)$ value and the spectroscopic quadrupole moment $Q_s(2_1^+)$ are related via the intrinsic quadrupole moment Q_0. The quadrupole

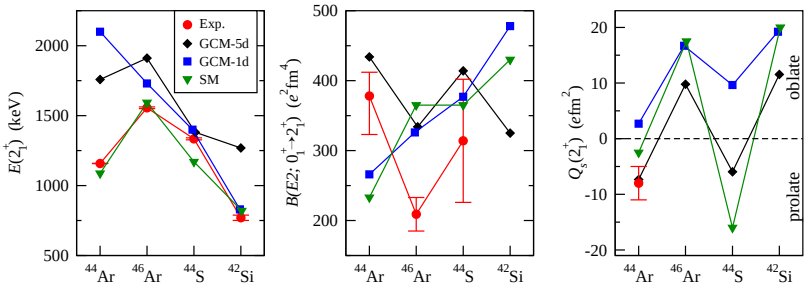

Figure 5. Excitation energies, $B(E2)$ values, and spectroscopic quadrupole moments for the 2_1^+ states in ^{44}Ar, ^{46}Ar, ^{44}S, and ^{42}Si. Experimental data for ^{44}Ar are taken from low-energy Coulomb excitation [117], for ^{46}Ar and ^{44}S from intermediate-energy Coulomb excitation [39, 113, 120], and for ^{42}Si from in-flight fragmentation [115]. The theoretical calculations (see text) are taken from [117].

moment extracted from the $B(E2)$ value using the rotational model is about twice as large as the measured quadrupole moment, showing that ^{44}Ar is not a rotational nucleus.

The results from low-energy Coulomb excitation of ^{44}Ar have been compared to both shell model calculations and to mean-field based configuration mixing calculations using the generator coordinate method (GCM) [117]. Figure 5 shows the comparison for excitation energies, $B(E2)$ values, and spectroscopic quadrupole moments of the 2_1^+ states in ^{44,46}Ar, ^{44}S, and ^{42}Si. The shell model calculations used the $sd-pf$ valence space and the SDPF-U interaction [116] with effective charges of $\epsilon_\pi = 1.35e$ and $\epsilon_\nu = 0.35e$. Figure 5 shows furthermore the results from two types of configuration mixing calculations: angular momentum projected GCM calculations with the axial quadrupole deformation as generator coordinate (labeled GCM-1d) [117, 119] and a five-dimensional approach using the GCM with Gaussian overlap approximation and considering both axial and triaxial quadrupole deformation (GCM-5d) [12, 117]. Both GCM calculations used the same Gogny D1S interaction [121, 122]. While the shell model calculations reproduce the excitation energies of the 2_1^+ states well throughout the region, the mean-field based approaches find too high energies for the less deformed nuclei. None of the calculations is able to reproduce the relatively low $B(E2)$ value for ^{46}Ar from intermediate-energy Coulomb excitation [39]. It should be noted, however, that a much larger value of $B(E2; 0_1^+ \rightarrow 2_1^+) = 560(210)\ e^2\text{fm}^4$ was found in a recent lifetime measurement for ^{46}Ar [123]. The measured quadrupole moment for ^{44}Ar is in good agreement with the triaxial configuration-mixing calculations, whereas the calculations restricted to axial shapes seem to be biased toward oblate shapes [117]. The different theoretical predictions for the quadrupole moment of the 2_1^+ state in ^{44}S vary considerably. This can be related to the expected prolate-oblate shape coexistence, which makes the quadrupole moment a very sensitive probe for configuration mixing in the wave function of this state. A reorientation measurement of the quadrupole moment via low-energy Coulomb excitation of ^{44}S would therefore represent a sensitive test of the theoretical models.

5.4. The Ni region from N=40 to N=50

The chain of nickel isotopes is one of the most varied to be found across the nuclear chart. It contains the three magic neutron numbers 20, 28, and 50, which are of particular interest, *e.g.* with ^{48}Ni as an example for two-proton radioactivity [124], ^{56}Ni a self-conjugate $N = Z$ nucleus, and ^{78}Ni a waiting-point in the astrophysical rapid neutron capture process [125]. The isotope ^{68}Ni has a high-lying 2_1^+ state [126], which suggests a sub-shell closure at $N = 40$. Mass measurements, on the other hand, suggest that the $N = 40$ shell gap is only weak [127, 128]. The $B(E2; 0_1^+ \rightarrow 2_1^+)$ value in ^{68}Ni was first measured using intermediate-energy Coulomb excitation and was found to be small [129]. It has been argued that the small $B(E2)$ value indicates not necessarily a large shell gap, but that it instead reflects the character of the 2_1^+ state as a predominant neutron excitation [130]. The ^{68}Ni nucleus was also studied in low-energy Coulomb excitation at ISOLDE, which confirmed the small $B(E2)$ value [131]. Details of the experiment are included in table 2, which summarizes all low-energy Coulomb excitation experiments in this mass region. An interesting technical detail of the ISOLDE experiment was the suppression of ^{68}Ga beam contaminants by utilizing the time structure of the proton driver accelerator and the different release times of Ni and Ga atoms in the production target [131].

Significant modifications of the shell structure are expected when neutrons start filling the $\nu g_{9/2}$ orbital due to the proton-neutron monopole term and and the tensor force [132]. Shell model calculations predict a decrease of the $\pi f_{5/2}$ and an increase of the $\pi f_{7/2}$ single-particle energies, leading to a reduction of the $Z = 28$ shell gap and increased collectivity. The $B(E2; 0_1^+ \rightarrow 2_1^+)$ value in ^{70}Ni, measured by intermediate-energy Coulomb excitation [133], shows indeed enhanced collectivity and is believed to contain an important contribution from proton excitations across the $Z = 28$ shell gap.

More information about the shell structure around ^{68}Ni comes from studies of the odd-mass copper isotopes. With the unpaired proton in the $\pi p_{3/2}$ orbital, the ground state of the copper isotopes has spin-parity $3/2^-$, and the lowest excited states have $J^\pi = 1/2^-$, $5/2^-$, and $7/2^-$, respectively. Coulomb excitation of the stable isotopes ^{63}Cu and ^{65}Cu has found these states to be rather collective [134], which led to the interpretation that the states are based on the coupling of the $p_{3/2}$ valence proton to the 2_1^+ state in the respective Ni core. A sharp decrease in the excitation energy of the $5/2^-$ states was observed in ^{71}Cu and ^{73}Cu after β decay and explained by the monopole migration of the $\pi f_{5/2}$ orbital [135, 136].

The odd-mass isotopes from ^{67}Cu to ^{73}Cu were studied using low-energy Coulomb excitation at ISOLDE [137]. Details of the experiment are included in table 2. Using resonant laser ionization the otherwise overwhelming beam contamination of Ga isobars could be largely reduced. In the heaviest isotope under study, ^{73}Cu, the known $5/2^-$ and $7/2^-$ states were populated in addition to a previously unobserved low-lying state at 135 keV, which was assigned $J^\pi = 1/2^-$. A corresponding state was also identified in ^{71}Cu at 454 keV, and three $B(E2)$ values, from the $1/2^-$, $5/2^-$, and $7/2^-$ states to the $3/2^-$ ground state, respectively, were measured in all four isotopes. The results are summarized in figure 6a. The $7/2^-$ states had been interpreted as the coupling of the $p_{3/2}$ proton to the 2_1^+ state in the Ni core [138]. The measured $B(E2; 3/2^- \rightarrow 7/2^-)$ values follow very closely the $B(E2; 0^+ \rightarrow 2^+)$ values in the corresponding Ni isotopes and confirm this interpretation. The $B(E2; 3/2^- \rightarrow 5/2^+)$ values are small in the neutron-rich isotopes and are consistent with a single-particle

Table 2. Summary of low-energy Coulomb excitation experiments in the region between $N = 40$ and $N = 50$. Experiments with Ge beams have been performed at HRIBF, all others at ISOLDE.

Nuclide	Energy (A MeV)	Intensity (s^{-1})	Purity %	Target	$B(E2;\uparrow)$ (e^2fm^4)	Ref.
^{68}Ni	2.90	10^4	68(1)	^{108}Pd	280^{+120}_{-100}	[131]
^{67}Cu	2.99	$1.2 \cdot 10^5$	97.5(7)	^{104}Pd	113(11),303(24),97(16)[a]	[137]
^{68}Cu	2.83	$3 \cdot 10^5$	74(2)[b]	^{120}Sn	68(6)[c]	[140]
^{69}Cu	2.99	$1.6 \cdot 10^5$	92.5(5)	^{104}Pd	87(8),76(8),155(24)[a]	[137]
^{70}Cu	2.83	$5 \cdot 10^4$	70(5)[d]	^{120}Sn	41(5)[c]	[140]
^{71}Cu	2.99	$2.3 \cdot 10^5$	65(1)	^{104}Pd	178(19),102(13),374(42)[a]	[137]
^{73}Cu	2.99	$8 \cdot 10^4$	17.4(2)	^{120}Sn	209(19),120(14),540(65)[a]	[137]
^{74}Zn	2.87	$3.0 \cdot 10^5$	83(4)	^{120}Sn	2010(160)	[144]
^{76}Zn	2.83	$1.1 \cdot 10^5$	73(7)	^{120}Sn	1450(180)	[144]
^{78}Zn	2.87	$4.3 \cdot 10^3$	64(13)	^{108}Pd	770(190)	[144]
^{80}Zn	2.79	$3.0 \cdot 10^3$	43(5)	^{108}Pd	730(150)	[144]
^{78}Ge	2.24	$1.4 \cdot 10^6$	57.1	^{nat}C	2220(140)	[149]
^{80}Ge	2.24	$1.4 \cdot 10^5$	95.3	^{nat}C	1390(270)	[149]
^{82}Ge	2.68	$5.5 \cdot 10^4$	19.2	^{48}Ti	1150(200)	[149]

[a] $B(E2;3/2^- \rightarrow 1/2^-)$, $B(E2;3/2^- \rightarrow 5/2^-)$, $B(E2;3/2^- \rightarrow 7/2^-)$
[b] isotopic purity, 86(3)% of ^{68}Cu in isomeric 6^- state
[c] $B(E2;6^- \rightarrow 4^-)$
[d] isotopic purity, 85(5)% of ^{70}Cu in 6^- ground state

character of this state. This finding together with the sharp drop in excitation energy gives a strong indication for the lowering of the $\pi f_{5/2}$ state as the $\nu g_{9/2}$ shell is filled. This monopole migration leads to an inversion of the ground-state spin for ^{75}Cu, which was experimentally established using laser spectroscopy [139]. The excitation energy of the $1/2^-$ states follows closely that of the $5/2^-$ states. However, the large $B(E2;3/2^- \rightarrow 1/2^-)$ values are incompatible with an interpretation as single-particle states. Their trend is also different from the neighboring Ni isotopes, so that an interpretation as particle-core coupled states was also rejected. Instead it was suggested that the $1/2^-$ states are based on a low-lying collective mode [137], which might also be related to the enhanced core polarization that was observed in ^{70}Ni [133].

Further understanding of the proton-neutron interaction and the stability of the shell gaps can come from studies of odd-odd nuclei around ^{68}Ni. In a pioneering experiment at ISOLDE, Stefanescu *et al* have used for the first time isomeric beams to measure transition rates in the odd-odd Cu isotopes ^{68}Cu and ^{70}Cu [140]. The low-lying structure of these nuclei is governed by the unpaired proton in the $\pi p_{3/2}$ orbital and one neutron particle or hole in the $\nu p_{1/2}$ or $\nu g_{9/2}$ orbitals, leading to $(1^+, 2^+)$ and $(3^-, 4^-, 5^-, 6^-)$ multiplets. In ^{68}Cu the 6^- member of the multiplet forms an isomeric state which has a longer half-life ($T_{1/2} = 3.75$ min) than the 1^+ ground state with $T_{1/2} = 31$ s. In ^{70}Cu, on the other hand, the ground state has $J^\pi = 6^-$, while the 3^- and 1^+ states form β-decaying isomers [141]. The proton-induced fission reactions in the uranium carbide target produced odd-odd Cu isotopes both in their ground state and in isomeric states. By scanning the frequency of a narrow-band laser for the first excitation in a two-step resonant ionization scheme, Cu atoms in either the nuclear ground state or excited isomeric states could be selectively ionized due to the different hyperfine splitting [142]. In this way it was possible to produce for the first

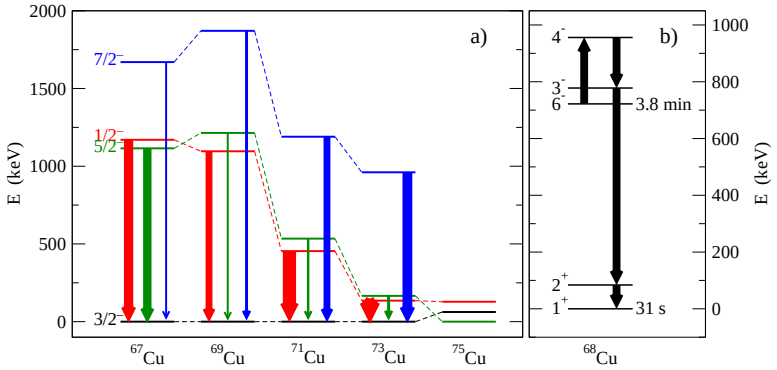

Figure 6. a) Systematics of low-lying states in odd-mass, neutron rich Cu isotopes. The arrows show the transitions which were observed in the Coulomb excitation experiment [137]; their width is proportional to the $B(E2)$ values in Weisskopf units. b) De-excitation of the 6^- isomer in ^{68}Cu via Coulomb excitation of the 4^- state [140].

time post-accelerated isomeric beams with the properties given in table 2.

The Coulomb excitation of the isomeric ^{68}Cu beam populated the 4^- state, which then decayed via the 3^- and 2^+ states to the 1^+ ground state, bypassing the 6^- isomer (figure 6b). The Coulomb excitation of the isomeric state in ^{68}Cu therefore constitutes an induced instantaneous release of energy stored in a nuclear isomer. The $B(E2; 6^- \rightarrow 4^-)$ values for ^{68}Cu and ^{70}Cu were extracted by normalizing the observed yields for projectile and target excitation and taking into account the isomeric ratios. In ^{72}Cu the 6^- state is located above the 4^- state, and the $B(E2)$ value is known from lifetime measurements [143]. Comparing the results for ^{70}Cu with shell model calculations, it was concluded that a single proton and neutron outside the $Z = 28$ and $N = 40$ (sub-)shell closures are not sufficient to polarize the ^{68}Ni core. The larger $B(E2)$ values in ^{68}Cu and ^{72}Cu, on the other hand, show the importance of proton excitations across the $Z = 28$ gap [140].

With two protons outside the $Z = 28$ shell the chain of neutron-rich Zn isotopes is ideally suited to study the evolution of the proton shell gap and the stability of the neutron (sub-)shell closures at $N = 40$ and 50, respectively. The even-even isotopes from ^{74}Zn up to ^{80}Zn have been Coulomb excited at low energy in experiments at ISOLDE [144, 145]. The excitation energy of the 2_1^+ states in ^{80}Zn was established for the first time in this experiment, and $B(E2; 0_1^+ \rightarrow 2_1^+)$ values were measured for all four isotopes. In the case of ^{74}Zn and ^{76}Zn two-step excitation to the 4_1^+ state was observed and $B(E2; 2_1^+ \rightarrow 4_1^+)$ values were also extracted. Experimental details are given in table 2, and γ-ray spectra following the Coulomb excitation of ^{80}Zn are shown in figure 7. Resonant laser ionization was used to selectively ionize the Zn atoms. The beam purity was further improved by equipping the target-ion source unit with a quartz transfer line which selectively trapped alkali atoms [148]. Isobaric Ga and Rb contaminants were nevertheless present in the beam. The beam composition was monitored by periodically switching the lasers on and off. The measurement for ^{80}Zn was at the limit of feasibility due to the short half live of only 545(16) ms, which caused decay losses during trapping and charge breeding of the ions. The $B(E2)$ values, which were extracted relative to the target excitation, are given in table 2 and

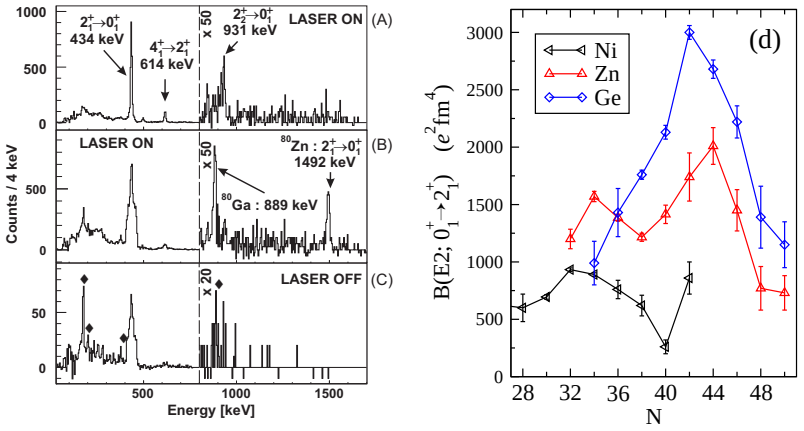

Figure 7. γ-ray spectra following Coulomb excitation of ^{80}Zn on a ^{120}Sn target [145]. (a) laser on and Doppler correction for target nuclei, (b) laser on and Doppler correction for projectiles, (c) laser off and Doppler correction for projectile. (d) $B(E2)$ values for the chains of Ni [19, 129, 133], Zn [133, 144, 145, 146, 147], and Ge [19, 149] isotopes.

compared to the $B(E2)$ values in neutron-rich Ni and Ge isotopes in figure 7.

The influence of the diagonal $\langle 2_1^+||E2||2_1^+\rangle$ matrix element could not be disentangled from that of the transitional $\langle 2_1^+||E2||0_1^+\rangle$ matrix element in this integral measurement of the Coulomb excitation probability, and the $B(E2)$ values were extracted under the assumption that $Q_s(2_1^+) = 0$. Slightly prolate quadrupole moments have been measured in electron scattering experiments for the stable Zn isotopes [150]. If the quadrupole moments in the neutron-rich Zn isotopes had similar magnitudes, the $B(E2)$ values extracted from the Coulomb excitation probabilities would change up to 15%. It would be possible to eliminate this systematic error by measuring the lifetimes of the 2_1^+ states in the neutron-rich even-even Zn isotopes, which would in turn also allow extracting the quadrupole moments from the Coulomb excitation data. Despite this uncertainty the $B(E2)$ values reveal an increased collectivity due to the filling of the $\nu 1g_{9/2}$ orbital. Proton-neutron correlations clearly dominate over the effect of a potential sub-shell closure at $N = 40$. The drop of the $B(E2)$ values toward ^{80}Zn, on the other hand, gives no indication for a breaking of the shell closure at $N = 50$. The results are well reproduced by large-scale shell model calculations. However, large effective charges are required, indicating a strong $Z = 28$ core polarization [144, 145].

The collectivity of neutron-rich Ge isotopes up to $N = 50$ was studied in low-energy Coulomb excitation experiments at HRIBF [149]. The purity of the Ge beams was significantly improved by extracting GeS^+ sulfide molecules from the UC_2 production target [69]. The beam composition and contamination with Se, As, and Ga isotopes was monitored using a Bragg detector and by detecting x-rays [151] emitted by the projectiles after stopping downstream from the Coulomb excitation setup. The $B(E2)$ values were extracted by normalizing the Coulomb excitation to the cross section for Rutherford scattering. In the case of ^{82}Ge the germanium detectors of the CLARION array were replaced by more efficient BaF_2 detectors, and the $B(E2)$ value was extracted relative to the known $B(E2)$ value of the ^{82}Se beam contaminant. The results are given in table 2 and shown together with the $B(E2)$ values for Ni and

Zn isotopes in figure 7. The lighter Ge isotopes are characterized by the coexistence of spherical and deformed configurations, in particular for ^{72}Ge [152]. The overall collectivity increases to a maximum for $N = 42$ and drops toward $N = 50$. This result is coherent with the behavior of the neutron-rich Zn and Se isotopes and confirms again the fragility of the $N = 40$ and the persistence of the $N = 50$ (sub-)shell closures, respectively.

5.5. Shape transitions and shape coexistence in Se and Kr isotopes near N=Z

The proton-rich Se and Kr isotopes near the $N = Z$ line are considered some of the best examples for shape coexistence in nuclei. The competition of prolate and oblate shapes can be understood from the existence of large deformed shell gaps in the single-particle spectra for proton and neutron numbers 34, 36, and 38, which are found both for prolate and oblate values of quadrupole deformation. Various theoretical models describe shape coexistence in this region of the nuclear chart [8, 153, 154, 155, 156, 157]. While there is a general consensus between these calculations that prolate and oblate shapes coexist, they differ in many details such as the excitation energy and quadrupole moment of the shape-coexisting states, and the transition rates between them. These observables are very sensitive to the degree of shape mixing, and their measurement represents consequently a stringent test of the models.

The first firm experimental proof for shape coexistence in the light Kr isotopes was the observation of low-lying excited 0^+ states in ^{74}Kr [158, 159] and ^{72}Kr [160]. These excited 0^+ states have relatively long lifetimes and can be interpreted as *shape isomers*. The excitation energy of the 0_2^+ state in ^{74}Kr is the lowest in the chain of Kr isotopes, while the electric monopole strength $\rho^2(E0)$ is the largest, which suggests a strong shape mixing in this nucleus. This observation led to the interpretation that prolate shapes are favored in the heavier isotopes ^{76}Kr and ^{78}Kr, with oblate shapes lower in energy in ^{72}Kr, and both shapes nearly degenerate in ^{74}Kr [160].

Clément *et al* have confirmed this scenario in pioneering low-energy Coulomb excitation experiments [161] at the SPIRAL facility at GANIL. Neutron-deficient Kr isotopes were produced by fragmentation of an intense ^{78}Kr primary beam on the carbon production target of SPIRAL. Quasi-pure secondary beams of ^{74}Kr and ^{76}Kr were accelerated in the CIME cyclotron to energies of 4.7 and 4.4 MeV per nucleon, respectively. The average intensity was 10^4 ions per second for ^{74}Kr and $5 \cdot 10^5$ for ^{76}Kr. In both cases a ^{208}Pb target was used for the Coulomb excitation. States up to $I^\pi = 8^+$ in the ground-state bands and several non-yrast states in ^{74}Kr and ^{76}Kr were populated in multiple steps. An example spectrum from the Coulomb excitation experiment with ^{74}Kr beam is shown in figure 8. The excitation probability of the various states was measured as a function of the scattering angle by dividing the data into several sub-sets for different ranges of scattering angles measured by a highly segmented annular silicon detector. More than 20 matrix elements, both transitional and diagonal, were needed to describe the population of the various states. The matrix elements were extracted from the observed γ-ray yields in a multi-dimensional fit using the code GOSIA.

The analysis of the Coulomb excitation data revealed inconsistencies with $B(E2)$ values from previous Doppler-shift lifetime measurements. The discrepancies could be resolved in a new lifetime measurement [162] using the RDDS technique. The precise lifetimes for states in the ground-state band in ^{74}Kr and ^{76}Kr from the complementary lifetime measurement were then used as additional constraints in the analysis of

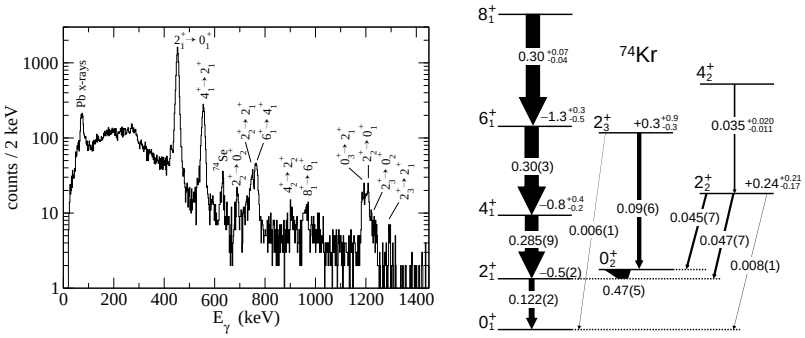

Figure 8. γ-ray spectrum following Coulomb excitation of ^{74}Kr. The resulting $B(E2)$ values for the respective transitions (in e^2b^2) and the spectroscopic quadrupole moments (in eb) for several states are shown in the level scheme on the right-hand side.

the Coulomb excitation cross sections, leading to an improved sensitivity for the transitional matrix elements to the non-yrast states and in particular for the diagonal matrix elements [161]. In this way it was possible to extract about 15 transitional and five diagonal matrix elements in each of the two isotopes. The resulting $B(E2)$ values and spectroscopic quadrupole moments for ^{74}Kr are included in figure 8. The sign of the spectroscopic quadrupole moments for the various states in ^{74}Kr and ^{76}Kr give firm experimental proof of prolate shapes for the states in the ground-state band of both isotopes, while excited 2^+ states could be associated with oblate shapes [161]. The experiments on ^{74}Kr and ^{76}Kr were the first to exploit the reorientation effect in Coulomb excitation with radioactive beams, *i.e.* they were the first to directly measure the shape of a radioactive nucleus in a short-lived excited state. They are also by far the most comprehensive Coulomb excitation studies with RIB so far. With the extensive sets of matrix elements for ^{74}Kr and ^{76}Kr, the nuclear shape could also be described in a model-independent way using rotational invariant products of the $E2$ operator [161].

The analysis of the matrix elements confirms a strong shape mixing in ^{74}Kr. A consequence of the strong mixing near the ground state is for example the relatively small $B(E2; 2_1^+ \rightarrow 0_1^+)$ value compared to the transitions higher in the ground-state band. The results support the interpretation of a shape inversion occurring between ^{74}Kr and ^{72}Kr. The relatively small $B(E2; 0^+ \rightarrow 2^+)$ value measured in ^{72}Kr using intermediate-energy Coulomb excitation [163] is consistent with oblate shape. A firm experimental proof for the shape of ^{72}Kr, however, has to await a measurement at low energy. The comparison of experimental $B(E2)$ values and quadrupole moments for ^{74}Kr and ^{76}Kr with configuration mixing calculations beyond the mean-field approach [8, 161] shown that it is crucial to include the triaxial degree of freedom in the calculations in order to achieve a correct description of prolate-oblate shape coexistence in this mass region [156].

Coexistence of prolate and oblate shapes is also expected in the neutron-deficient Se isotopes. Based on its rotational properties, the ground-state band in the $N = Z$ nucleus ^{68}Se was interpreted as a rare example for oblate rotation [164]. The excited rotational band with larger moment of inertia is understood in this scenario as a prolate rotational band. Contrary to the case of the light Kr isotopes, however, no

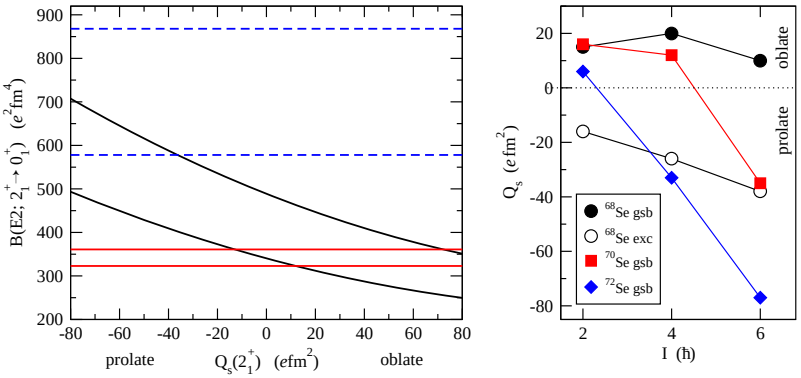

Figure 9. $B(E2; 2_1^+ \rightarrow 0_1^+)$ value as a function of the spectroscopic quadrupole moment $Q_s(2_1^+)$ for ^{70}Se. The sloping lines indicate the 1σ limit from the Coulomb excitation data [166]. The dashed (blue) and solid (red) horizontal lines represent the 1σ limits of the lifetime measurements of Heese [167] and Ljungvall [168], respectively. The graph on the right-hand side shows theoretical quadrupole moments for the ground-state bands in ^{68}Se, ^{70}Se, and ^{72}Se and for the excited band in ^{68}Se [168].

low-lying excited 0^+ state was observed despite much effort [165]. The moment of inertia of the ground-state band in ^{70}Se is at low spin very similar to that of the ground-state band in ^{68}Se; at higher spin the band follows very closely the excited band in ^{68}Se. Using the same arguments as for ^{68}Se, the behaviour of ^{70}Se could be understood as a transition from oblate shape near the ground state to prolate shape at higher excitation energy and higher angular momentum.

To answer the question whether well-deformed oblate shapes are found near the ground-state of ^{70}Se, a low-energy Coulomb excitation experiment was performed at ISOLDE [166]. A particularity of the experiment was the extraction of ^{70}Se from the ZrO_2 production target in form of a $^{70}Se^{12}C^{16}O^+$ selenium carbonyl molecule. The molecule was broken up in the intense electron beam of the charge-state booster REXEBIS after an initial mass separation for $A = 98$. In this way the contamination of the beam with $A = 70$ isobars was avoided, and a quasi-pure beam of ^{70}Se was accelerated to an energy of 2.94 MeV per nucleon with an intensity of 10^4 ions per second. Due to the relatively low energy of the beam, the Coulomb excitation cross section was low, and only the 2_1^+ state was populated. With the resulting low count rates, only the integrated cross section over all scattering angles was measured. The coupling to higher-lying states could be neglected under the conditions of the experiment. The total excitation probability to populate the 2_1^+ state, however, depended not only on the transitional matrix element $\langle 2_1^+ || E2 || 0_1^+ \rangle$, but also strongly on the diagonal matrix element $\langle 2_1^+ || E2 || 2_1^+ \rangle$. The two matrix elements were treated as unknown variables in an analysis using GOSIA. The ranges of the two matrix elements that are compatible with the observed excitation cross section of the 2_1^+ state can be visualized in a plot of the $B(E2; 0_1^+ \rightarrow 2_1^+)$ value against the spectroscopic quadrupole moment $Q_s(2_1^+)$, as shown in figure 9. It is not possible to determine both quantities from the integral Coulomb excitation cross section alone.

Since the $B(E2; 2_1^+ \rightarrow 0_1^+)$ value derived from the lifetime of the 2_1^+ state is

independent of the quadrupole moment, both quantities can be determined from complementary Coulomb excitation and lifetime measurements. The lifetime of the 2_1^+ state in ^{70}Se had been measured to be $\tau = 1.5(3)$ ps [167]. Combining the resulting $B(E2)$ value with the excitation probability found in the Coulomb excitation experiment (see figure 9), prolate shape was associated with the 2_1^+ state in ^{70}Se [166], contrary to expectations. A new, more precise measurement, however, found a much longer lifetime of $\tau = 3.2(2)$ ps for the 2_1^+ state in ^{70}Se [168]. The discrepancy between the two lifetime measurements was attributed to effects related to unobserved side feeding, which could affect the older γ-singles measurement, but not the new γ-γ coincidence measurement. The consequence of the lower $B(E2)$ value for the shape of ^{70}Se is also seen in figure 9: Only oblate shapes are consistent with both the Coulomb excitation and the new lifetime data [168]. This experimental result is now consistent with theoretical calculations, which predicted ^{70}Se to be oblate near the ground state. The right-hand part of figure 9 shows quadrupole moments from GCM configuration-mixing calculations [168], which predict a rapid transition from oblate to prolate shape within the ground-state band of ^{72}Se, a slower transition from oblate to prolate for ^{70}Se, and finally a true coexistence of oblate and prolate shapes for ^{68}Se. A future low-energy Coulomb excitation experiment for ^{68}Se would consequently be a most sensitive test of this scenario of shape transitions and shape coexistence.

5.6. Toward ^{100}Sn

Nuclei around ^{100}Sn are of key importance for the understanding of the nuclear shell structure. The ^{100}Sn nucleus has closed proton and neutron shells and is the heaviest self-conjugate nucleus; its protons and neutrons occupy the same orbitals, but have very different binding energies. As a consequence its structure may be influenced by proton-neutron pairing and by the coupling of the weakly bound protons to the continuum. The interaction between protons and neutrons in spin-orbit partner orbitals leads to the so-called monopole drift of the single-particle energies [169], which can change the ordering of the orbitals in exotic nuclei. The long chain of Sn isotopes provides the opportunity to study the evolution of the shell structure, and in particular the evolution of the proton gap, across a full major shell.

The energies of the 2^+ states in the Sn isotopes are almost constant between the shell closures at $N = 50$ and 82, which can be explained by the generalized seniority scheme [170]. The $B(E2; 0^+ \rightarrow 2^+)$ values, which are very sensitive to the size of the proton shell gap and a possible core polarization, are in the seniority scheme expected to follow a parabolic trend that peaks at mid-shell. Large-scale shell model calculations also predict a parabolic trend for the $B(E2)$ values [171]. Coulomb excitation is the only viable technique to measure $B(E2)$ values in the neutron-deficient Sn isotopes, since lifetime measurements are obstructed by the occurrence of isomeric 6^+ states with lifetimes in the nanosecond range, *i.e.* at least two orders of magnitude longer than the expected lifetimes of the 2^+ states.

The $B(E2; 0^+ \rightarrow 2^+)$ values have been measured in intermediate-energy Coulomb excitation experiments at GSI for ^{108}Sn [171] and at MSU for the chain of even-mass isotopes from ^{112}Sn down to ^{106}Sn [172]. Due to experimental difficulties, contributions from processes other than Coulomb excitation could not be completely ruled out in the measurement at MSU, so that in particular the value for ^{106}Sn had to be considered tentative [172]. In parallel to the measurements at intermediate energy, experiments have been performed at ISOLDE to measure $B(E2)$ values in neutron-

Table 3. Experimental details and results from low-energy Coulomb excitation experiments for Cd, and Sn isotopes performed at ISOLDE.

Nuclide	Energy (A MeV)	Intensity (s^{-1})	Purity %	Target	$B(E2;\uparrow)$ (e^2b^2)	Ref.
^{100}Cd	2.87	$3 \cdot 10^3$	100(10)	^{109}Ag	< 0.28	[179]
^{102}Cd	2.87	$5 \cdot 10^5$	99.6(1)	^{64}Zn,^{109}Ag	0.28(4)	[179]
^{104}Cd	2.87	$1 \cdot 10^6$	99.2(1)	^{64}Zn,^{109}Ag	0.33(3)	[179]
^{106}Sn	2.83	$3 \cdot 10^4$	29(4)	^{58}Ni	0.195(39)	[174]
^{108}Sn	2.82	$6 \cdot 10^5$	59(3)	^{58}Ni	0.222(19)	[174]
^{110}Sn	2.82	$9 \cdot 10^5$	90(1)	^{58}Ni	0.220(22)	[173]

deficient Sn isotopes using low-energy Coulomb excitation [173, 174]. Experimental details of the experiments are summarized in table 3. The Sn beams were produced using resonant laser ionization, and beam impurities were monitored by switching the lasers off periodically. Although beam impurities complicate the data analysis and are generally unwanted, in this particular case it was possible to extract additional information on the structure of odd-odd ^{106}In and ^{108}In, which were present in the beam as contaminants [175]. The $B(E2)$ values for the Sn isotopes were extracted relative to the target excitation probability using the known $B(E2)$ value for ^{58}Ni. Due to their semi-magic character it can be assumed that the Sn nuclei are spherical and have a spectroscopic quadrupole moment of $Q_s(2^+) \approx 0$. The results from both low-energy and intermediate-energy Coulomb excitation experiments are summarized in figure 10. Low-energy Coulomb excitation experiments have also been performed recently for the stable isotopes ^{114}Sn at GSI [176] and for ^{112}Sn at IUAC New Delhi [177] in order to reduce the uncertainties for the $B(E2; 0_1^+ \rightarrow 2_1^+)$ values in the lightest stable isotopes.

The totality of measurements clearly indicates a deviation from a parabolic trend of the $B(E2)$ values for the light Sn isotopes. Figure 10 also shows the results from two large-scale shell model calculations [171]. The first calculation, which used a neutron valence space outside a ^{100}Sn core and an effective charge of $\epsilon_\nu = 1.0e$, reproduces the $B(E2)$ values for the heavier Sn isotopes very well, but not the enhanced transition strength in the lighter isotopes. It is natural to assume that the enhancement for the lighter isotopes is related to excitations of the core. The second calculation, which used a valence space for protons and neutrons outside a ^{90}Zr core and effective charges of $\epsilon_\pi = 1.5e$ and $\epsilon_\nu = 0.5e$, shows that the $B(E2)$ strength increases when proton excitations across the $Z = 50$ shell closure are included [171]. However, a seniority truncation was applied to keep the calculation with ^{90}Zr core feasible, which imposes a parabolic trend for the $B(E2)$ values. Figure 10 compares the experimental data also to relativistic QRPA calculations [178]. In this approach it is not necessary to assume an inert core or effective charges, and the parametrization of the Hamiltonian is universally valid across the nuclear chart. Considering that there are no free parameters to adjust, the agreement with experimental data is satisfactory, and in particular the calculation reproduce an enhancement of the $B(E2)$ strength for the Sn isotopes with $A \leq 114$.

To learn more about the role of residual nucleon-nucleon interactions in the ^{100}Sn region, low-energy Coulomb excitation has also been studied at ISOLDE for ^{100}Cd, ^{102}Cd, and ^{104}Cd [179]. High beam purities were achieved using resonant laser ionization and a quartz transfer line for the target-ion source system [180].

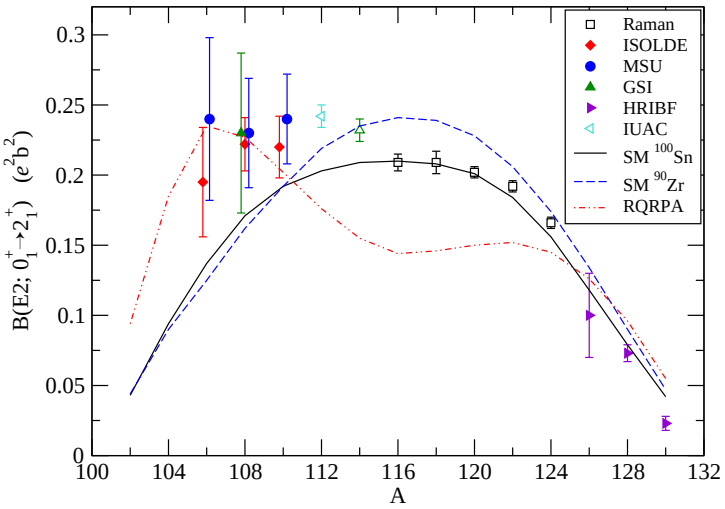

Figure 10. Experimental and theoretical $B(E2)$ values for the chain of even-even Sn isotopes between the $N = 50$ and $N = 82$ shell closures. Data for the stable isotopes (open symbols) are taken from the compilation of Raman [19] and recent measurements from GSI [176] and IUAC New Delhi [177]. Data for the neutron-rich isotopes are from HRIBF [188] (see section 5.7). Measurements for the neutron-deficient isotopes were performed in different energy regimes at ISOLDE [173, 174], MSU [172], and GSI [171]. The results are compared to shell model calculations [171] using either a ^{100}Sn or ^{90}Zr core, and to relativistic QRPA calculations [178].

Details of the experiments are included in table 3. The γ-ray yields for the $2_1^+ \rightarrow 0_1^+$ transition in ^{102}Cd and ^{104}Cd were measured for two angular ranges with a ^{64}Zn target, and an additional yield was measured with a ^{109}Ag target. The excitation cross sections were normalized using the known matrix elements for the target nuclei. The transitional $\langle 2_1^+||E2||0_1^+\rangle$ and diagonal $\langle 2_1^+||E2||2_1^+\rangle$ matrix elements for the projectiles were extracted from the γ-ray yields using a maximum likelihood approach [179]. The resulting $B(E2)$ values are included in table 3. The quadrupole moments were found to be $Q_s(2_1^+) = +0.22 \pm 0.11(\text{stat}) \pm 0.15(\text{sys})$ for ^{102}Cd and $Q_s(2_1^+) = +0.06 \pm 0.10(\text{stat}) \pm 0.11(\text{sys})$ for ^{104}Cd. The systematic errors are mostly related to the uncertainty of the matrix elements for the target nuclei. The $B(E2)$ values for ^{102}Cd and ^{104}Cd were also determined in a RDDS lifetime measurement [181]. There is good agreement for the $B(E2)$ value in ^{102}Cd obtained in the lifetime and Coulomb excitation measurements, and consequently the quadrupole moment does not change significantly when the $B(E2)$ value from the lifetime measurement is considered in the analysis of the Coulomb excitation data. For ^{104}Cd, however, the $B(E2)$ value from the lifetime measurement is somewhat larger than the one found in Coulomb excitation. If this larger $B(E2)$ value is used to constrain the Coulomb excitation analysis, a larger negative spectroscopic quadrupole moment is required to reproduce the excitation cross section, an effect similar to the one observed for ^{70}Se (see figure 9). Only an upper limit could be determined for the $B(E2)$ value in ^{100}Cd from Coulomb excitation on a ^{109}Ag target. In a comparison with shell model calculations, the best agreement was found when the neutron effective charge

Table 4. List of Coulomb excitation experiments with RIB around ^{132}Sn. Experiments with Cd and Xe beams have been performed at ISOLDE, those with Sn and Te beams at HRIBF.

Nuclide	Energy (A MeV)	Intensity (s^{-1})	Purity %	Target	$B(E2;\uparrow)$ (e^2b^2)	Ref.
^{122}Cd	2.85	10^4	70	^{108}Pd	0.37(11)	[191, 193]
^{124}Cd	2.85	10^4	38	^{64}Zn, ^{104}Pd	0.35(6)	[191, 193]
^{126}Cd	2.85	10^4	75	^{64}Zn	0.22(6)	[193]
^{126}Sn	3.0	10^7	50	^{nat}C	0.10(3)	[189, 188]
^{128}Sn	3.0	$3 \cdot 10^6$	>99[a]	^{nat}C	0.073(6)	[189, 188]
^{130}Sn	3.0	$5 \cdot 10^5$	>99[a]	^{nat}C	0.023(5)	[189, 188]
^{132}Sn	3.56, 3.75	10^5	96	^{48}Ti	0.11(3)	[190, 188]
^{134}Sn	2.99	$9 \cdot 10^3$	25.6(2)	^{90}Zr	0.029(5)	[190, 188]
^{132}Te	2.65, 3.0	10^7	86(4)	^{nat}C	0.172(17)	[186]
^{132}Te	2.65	10^6	81(2)	^{nat}C	0.19(3)	[187]
^{134}Te	2.96	$2 \cdot 10^6$	87(4)	^{nat}C	0.096(12)	[186]
^{134}Te	2.61	10^5	44(2)	^{nat}C	0.13(4)	[187]
^{136}Te	2.91	10^5	59(5)	^{nat}C	0.103(15)	[186]
^{138}Xe	2.84	10^5	100	^{96}Mo	0.38(10)	[192, 193]
^{140}Xe	2.84	10^5	100	^{96}Mo	0.52(10)	[192, 193]
^{142}Xe	2.84	10^5	100	^{96}Mo	0.69(10)	[192, 193]
^{144}Xe	2.7	?	100	^{96}Mo	0.73(18)	[193]

[a] $\sim$10% in metastable 7^- state.

was increased from $\epsilon_\nu = 1.07e$ in ^{104}Cd to $1.27e$ in ^{102}Cd, while keeping the proton effective charge constant at $\epsilon_\pi = 1.6e$ [179]. This suggests the presence of a small enhancement of the transition strengths when approaching $N = 50$, however, less pronounced than for the Sn isotopes.

5.7. $N = 82$ and beyond: the region around ^{132}Sn

At the other extreme of the chain of Sn isotopes lies ^{132}Sn, the heaviest neutron-rich nucleus with closed proton and neutron shells, which is of particular importance for the investigation of the nuclear shell structure in neutron-rich nuclei. In addition to the interest for nuclear structure, the $N = 82$ isotones below ^{132}Sn are also crucial for the understanding of nucleosynthesis via the rapid neutron capture process. A reduction of the $N = 82$ shell gap below ^{132}Sn could for example explain deficiencies in r-process abundance calculations [182]. Nuclei in the vicinity of ^{132}Sn are strongly produced in the fission of actinides, and information on their structure can be obtained by fission-fragment spectroscopy. In favorable cases it is possible to measure lifetimes of excited states in mass separated fission fragments by applying fast timing techniques [183]. However, this method is limited to relatively long-lived states with lifetimes above $\sim$10 ps. Picosecond lifetimes in fission fragments have also been measured using variants of the RDDS [184] and DSA [185] techniques in combination with spontaneous fission of ^{252}Cf and ^{248}Cm samples, respectively.

With the availability of re-accelerated fission fragment beams at HRIBF and ISOLDE, low-energy Coulomb excitation experiments to study the collectivity of nuclei around ^{132}Sn became feasible. A summary of the experimental efforts and results is presented in table 4. First pioneering experiments were performed by Radford *et al* at HRIBF investigating the collectivity of Te isotopes at and beyond the $N = 82$ shell closure [186]. The ^{132}Te, ^{134}Te, and ^{136}Te projectiles were Coulomb excited

on a natural carbon target at energies around 3 MeV per nucleon. The detection of scattered target nuclei in the CsI crystals of the HyBall detector at forward angles served both as a clean trigger to suppress background from the decay of the radioactive beam and for the normalization to the Rutherford cross section. The exact beam composition was monitored by measuring γ rays following the β decay of stopped beam particles and by measuring characteristic x rays produced in various foils placed downstream from the carbon target. Transitions originating from stable Ba isobars were visible in the Coulomb excitation spectra for the $A = 134$ and $A = 136$ experiments, so that their intensity could be determined from the known $B(E2)$ values. The $B(E2; 0_1^+ \rightarrow 2_1^+)$ values for the Te isotopes were extracted by comparing the γ-ray yields measured with the CLARION array with Coulomb excitation calculations using the Winther-de Boer code. Coulomb excitation of ^{132}Te and ^{134}Te was also performed at HRIBF with a different detector setup involving an annular NaI and micro-channel plate detectors [187].

Measurements of $B(E2)$ values were also performed for the even-mass Sn isotopes between ^{126}Sn and ^{134}Sn at HRIBF [188, 189, 190]. The radioactive Sn isotopes were extracted from the production target as SnS^+ sulfide molecules, which greatly improved the purity of the beams [68]. For the isotopes up to ^{130}Sn the setup comprising the HyBall charged-particle and CLARION γ-ray detectors was used. The measurement for ^{132}Sn posed greater difficulties, since the excitation energy of the 2_1^+ state lies above 4 MeV, leading to a very small Coulomb excitation cross section. This difficulty was overcome by using an array of 150 BaF_2 detectors with much higher efficiency than the CLARION detectors. To increase the cross section a ^{48}Ti target was used instead of carbon, and the beam energy was increased to 3.75 MeV per nucleon. The scattered particles were detected in an annular double-sided silicon detector, and the range of scattering angles was limited in the analysis to ensure safe Coulomb excitation. In case of ^{134}Sn, the main difficulty was related to the low intensity and purity of the beam.

Measurements for the chains of Cd and Xe isotopes were performed at ISOLDE [191, 192, 193]. For noble gases beam contaminations can be suppressed by using a cold plasma ion source, resulting in pure beams of Xe isotopes. Beam purification for the Cd isotopes was achieved by resonant laser ionization. All ISOLDE experiments used the same experimental setup comprising the segmented germanium detectors of the MINIBALL array and an annular DSSD. The results from the ISOLDE measurements have so far only been published in conference proceedings and some were labeled preliminary.

The measured $B(E2)$ values in the region around ^{132}Sn are given in table 4 and shown as a function of neutron number in figure 11. Two general trends are observed: The collectivity increases rapidly with the number of valence particles and holes outside ^{132}Sn, and the increase of the $B(E2)$ values is symmetric about the neutron number $N = 82$. The semi-magic Sn isotopes have the lowest $B(E2)$ values, as expected, and their trend as a function of neutron number is relatively flat. The collectivity increases faster for the chains of Te and Cd isotopes with two proton particles or holes outside the $Z = 50$ shell, respectively. The similarity of the $B(E2)$ values for the respective Cd and Te isotones illustrates the symmetry of proton particle and hole excitations. The chains of Xe and Ba isotopes with four and six valence protons, respectively, finally show a very rapid onset of collectivity which is symmetric about the neutron shell closure. There are, however, two exceptions from these general trends: The $B(E2)$ value for doubly-magic ^{132}Sn itself is larger than for

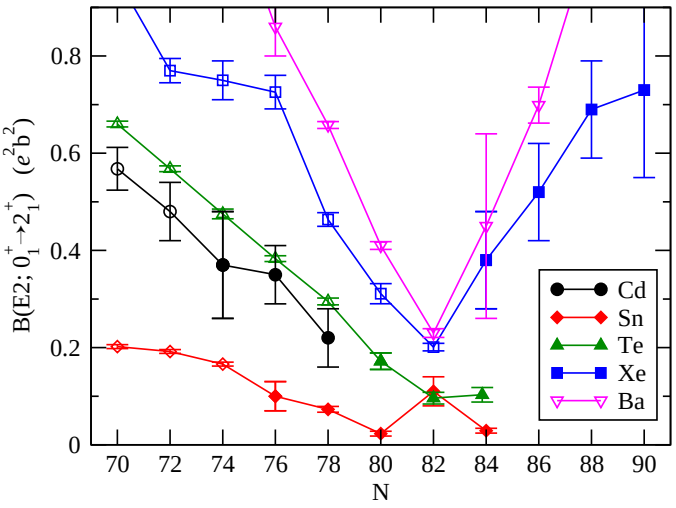

Figure 11. $B(E2)$ values in neutron-rich even-even nuclei around ^{132}Sn. Values obtained by Coulomb excitation with RIB from HRIBF (Sn, Te) and ISOLDE (Cd, Xe) are shown by filled symbols. All other values are taken from the compilation of Raman [19], except for $^{130-136}$Xe, where newer values are available [194].

neighboring Sn isotopes and is not the lowest of all, as one might naively expect, and the $B(E2)$ values for the Te isotopes are not symmetric about $N = 82$, with the value for ^{136}Te being much lower than the one for ^{132}Te.

The increase of the $B(E2)$ value for ^{132}Sn seems counterintuitive at first, but is easily explained. The 2_1^+ states in the Sn isotopes are dominated by neutron excitations. For ^{132}Sn, however, both proton and neutron excitations are hindered. The relative weight of the proton amplitude is therefore higher in ^{132}Sn compared to its neighbours, causing the local increase of the $B(E2)$ value. This effect, which is also observed *e.g.* for ^{208}Pb, is well described by QRPA calculations [195, 196, 197].

Shell model calculations reproduce the $B(E2)$ value for ^{134}Sn with an effective neutron charge of $\epsilon_\nu \approx 0.7e$ [198, 199, 200]. However, the shell model cannot explain the $B(E2)$ values in ^{134}Sn, ^{134}Te and ^{136}Te simultaneously. While the $B(E2)$ value for ^{134}Te can be reproduced with the usual effective proton charge of $\epsilon_\pi \approx 1.5$, the low value for ^{136}Te would require a much smaller effective charge of $\epsilon_\pi \approx 1.0$ [186, 199]. Monte Carlo shell model calculations have found a slightly better agreement, but still overestimated the $B(E2)$ value for ^{136}Te [201]. The unusual character of ^{136}Te is emphasized when the $B(E2)$ value is set in relation to the excitation energy of the 2_1^+ state. The fact that both the energy of the state and the $B(E2)$ value in ^{136}Te are reduced by about 40% compared to ^{132}Te is inconsistent with the empirical relation between energy and transition strength, which was first recognized by Grodzins [202]. The unexpected result for ^{136}Te was first explained by Terasaki *et al* [195] in QRPA calculations by a reduced neutron monopole pairing gap for ^{136}Te compared to ^{132}Te. As a result, the energy required for breaking a neutron pair to form the 2_1^+ state is reduced and the 2_1^+ state is found at a lower excitation energy in ^{136}Te. For the same reason the neutron amplitude in the wave function is increased compared to ^{132}Te, resulting in a smaller $B(E2)$ value. The effect is not visible in Xe and Ba isotopes where proton pairing and proton-neutron interactions become more important.

5.8. Shape coexistence in Hg and Pb isotopes near neutron mid-shell

The neutron-deficient Hg and Pb nuclei near $N \approx 104$ represent another prominent example of shape coexistence [203]. The first indication for shape coexistence in light Hg isotopes was observed in form of exceptionally large isotope shifts [204], indicating a significant change in the charge radius between ^{187}Hg and ^{185}Hg. Spectroscopy results (see [205] for a review) led to the interpretation of slightly oblate ground-state bands which are crossed by intruder bands with larger prolate deformation in the Hg isotopes with $A \leq 188$. Further evidence for shape coexistence in this mass region came from the observation of low-lying 0^+ states [206]. The perhaps most spectacular case is ^{186}Pb, where the three lowest states have spin-parity 0^+ and are interpreted as coexisting spherical, oblate, and prolate shapes [207]. The excited 0^+ states can be interpreted as *2p–2h* and *4p–4h* proton excitations across the $Z = 82$ shell gap [208]. The occurrence of oblate and prolate deformation in this region was first predicted by Nilsson-Strutinsky calculations [209]. More recently the shape coexistence in light Pb isotopes was described by GCM configuration mixing calculations using Skyrme [7] and Gogny [11] interactions.

A direct proof for the shape coexistence scenario in this mass region could come from low-energy Coulomb excitation experiments. Such experiments have been performed at ISOLDE using beams of ^{182}Hg, ^{184}Hg, ^{186}Hg, and ^{188}Hg [210]. Although the data analysis for these experiments is still in progress and results are only preliminary, the experiments shall nevertheless be mentioned, as they can be considered a milestone for Coulomb excitation studies with RIB. The experiments successfully demonstrate the possibility to produce and exploit heavy RIB for low-energy Coulomb excitation experiments. The Hg nuclides were produced in reactions of high-energy protons in a molten Pb target with subsequent ionization in a plasma ion source. After trapping charge states of 44+ and 45+ were produced in the REXEBIS charge state booster without significant losses. The beams were accelerated to 2.85 MeV per nucleon with intensities ranging from $5 \cdot 10^3$ per second for ^{182}Hg to $3 \cdot 10^5$ per second for ^{188}Hg. Secondary targets of ^{107}Ag, ^{112,114}Cd, or ^{120}Sn were used for the Coulomb excitation of the different Hg isotopes using the standard setup and technique employed at ISOLDE. In addition to the 2_1^+ state, which was populated in all Hg isotopes under study, the 4_1^+ state was excited in all isotopes except ^{186}Hg, and in addition the 2_2^+ state was populated in both ^{182}Hg and ^{184}Hg. Although data is still under analysis, it is clear that several transitional and diagonal matrix elements can be extracted. The experiment will hence yield direct information on the nuclear shape associated with individual states. In addition, information on the configuration mixing between the oblate and prolate bands can be extracted from the transitional matrix elements.

Similar to other cases of low-energy Coulomb excitation with RIB, also the study of light Hg isotopes benefits from complementary lifetime measurements [211, 212]. For the lightest isotopes ^{180}Hg and ^{182}Hg lifetimes have been measured recently by combining the recoil-distance Doppler shift and the recoil-decay tagging techniques [213, 214]. After the successful measurements for the light Hg isotopes Coulomb excitation experiments are now also being carried out at ISOLDE for neutron-deficient Pb and Po isotopes.

6. Summary and outlook

The examples discussed in section 5 illustrate the progress that has been achieved over the last decade in applying the 'old' technique of low-energy Coulomb excitation to exotic nuclei using new radioactive beam facilities. The scientific objectives of the studies can be roughly divided into two groups: (i) understanding how the nuclear shell structure changes in exotic nuclei with extreme proton-to-neutron ratio, and (ii) understanding the interrelation between the microscopic structure of the nucleons and the macroscopic nuclear shape, which can change rapidly with proton and neutron number and can lead to shape coexistence in some exotic nuclei. While in the first case the interest is directed toward measuring the collectivity of nuclei near the traditional or potentially new magic numbers, in the second case one aims at measuring observables related to the nuclear shape in open-shell nuclei. By providing electromagnetic transition strengths and quadrupole moments for exotic nuclei, low-energy Coulomb excitation with RIB is very well suited as a technique to address both questions. Electromagnetic matrix elements are a very sensitive probe of nuclear wave functions, so that low-energy Coulomb excitation measurements serve as a stringent test of theoretical nuclear structure models. The collectivity of nuclei in the vicinity of closed shells can be described using the nuclear shell model or extensions of the mean-field approach based on the (quasiparticle) random phase approximation. The generator coordinate method is another extension of the mean-field approach that is particularly well adapted to describe the collectivity and shape of deformed open-shell nuclei. The results of low-energy Coulomb excitation measurements in exotic nuclei have been very instrumental for testing and advancing these theoretical models.

For light and medium heavy nuclei, which can be produced in fragmentation reactions, Coulomb excitation at intermediate energy is an alternative technique to study nuclear collectivity. Such measurements are usually limited to the $B(E2)$ value of the first excited state, but in some cases it is possible to reach nuclei far from stability which are inaccessible using ISOL beams and low-energy Coulomb excitation. For nuclei which are produced in fission, low-energy Coulomb excitation with ISOL beams is a highly competitive technique to study even very exotic nuclei, as the examples of ^{80}Zn or several nuclei of the region around ^{132}Sn show. The possibility to use the ISOL technique to produce and accelerate even heavier nuclei such as Hg or Rn offers unique opportunities for studying shapes and collectivity in exotic nuclei. The combination of ISOL production and resonant laser ionization has proven to be very powerful to produce pure beams, and in some cases it is even possible to use the selectivity of laser ionization to produce beams of nuclei in an excited isomeric state.

Another uniqueness of low-energy Coulomb excitation is the possibility to measure quadrupole moments of short-lived excited states. The measurements in light Kr isotopes have demonstrated the potential to obtain comprehensive sets of both transitional and diagonal electromagnetic matrix elements in exotic nuclei. Experiments utilizing the reorientation effect to measure quadrupole moments are, however, very challenging. To accomplish reorientation measurements with low-intensity RIB often requires additional spectroscopic data obtained in complementary measurements. Of particular importance in this context are the lifetimes of excited states, as they only depend on transition strengths, but not on quadrupole moments. Measurements of lifetimes of excited states in the picosecond range have been extended to more exotic nuclei by combining the RDDS method with recoil-decay tagging or by using alternative reaction mechanisms such as multi-nucleon transfer or knock-out

reactions.

Low-energy Coulomb excitation experiments constitute an important aspect in the effort to explore exotic nuclei, and such experiments have contributed significantly to the success of the research programmes at ISOL-based RIB facilities. It will be possible to extend Coulomb excitation studies to even more exotic nuclei at the next-generation RIB facilities, which are presently under construction, and it can be expected that such experiments will play an equally prominent role in the scientific programmes of these facilities. Not only will the focus be shifted to nuclei even further away from the stability line, which are not accessible today, but it will also be possible to reach a larger number of states and matrix elements due to higher intensities of the RIB. Nuclei for which it is only possible today to measure the $B(E2; 0_1^+ \rightarrow 2_1^+)$ value can then be studied in more detail via multiple-step Coulomb excitation including the measurement of quadrupole moments by exploiting the reorientation effect.

Of the existing ISOL facilities, ISOLDE offers the widest range of beams, but experiments are limited by the maximum attainable beam energy of 3 MeV per nucleon and often by low beam intensities. The (high-intensity, high-energy) HIE-ISOLDE upgrade [215] will overcome many of the present limitations. In a first phase a new superconducting post-accelerator with a maximum energy of 10 MeV per nucleon will be built. In a second phase also the beam intensity and purity will be increased by using higher primary beam power and constructing a new high-resolution spectrometer. With the SPIRAL-2 project [216] a new ISOL facility is being built at GANIL. A new superconducting driver accelerator will deliver a deuteron beam of 200 kW power on a carbon converter and uranium carbide target to induce more than 10^{13} fission per second. The fission fragments will be accelerated in the existing CIME cyclotron. It is expected to achieve beam intensities of more than 10^6 ions per second for a wide range of fission fragments and up to 10^{10} ions per second for selected isotopes. HIE-ISOLDE and SPIRAL-2 can be seen as stepping stones toward the ultimate ISOL facility EURISOL [217]. The Facility for Rare Isotope Beams (FRIB) [17, 218] is a very advanced next-generation RIB accelerator under construction at Michigan State University. FRIB will use both ISOL and in-flight techniques to produce RIB. In addition to these major new facilities, several smaller ISOL accelerators are being built or planned around the world, increasing the availability of RIB.

With unprecedented intensities of RIB delivered by the new accelerators, experiments and in particular the detection systems will have to adapt to these new conditions. The new γ-ray tracking detector arrays AGATA [219] and GRETINA [220] are ideally suited for experiments with high-intensity RIB. These instruments can sustain very high count rates due to the segmentation of the germanium detectors and their digital signal processing electronics. At the same time they have very high resolution and efficiency due to the position sensitivity of the detectors and the tracking of individual gamma rays through a shell of closely packed detectors [221]. With the new RIB facilities on the horizon, and with the advances in detector technology and experimental technique, it can be expected that low-energy Coulomb excitation experiments will continue to play an important role in the fascinating exploration of exotic nuclei.

Acknowledgments

The work described in this review would not have been possible without the development work and continuous improvements carried out by the technical staff at the various laboratories and their support during experimental campaigns.

References

[1] Bohr A and Mottelson B 1975 *Nuclear Structure* Vol.II (Reading: W.A. Benjamin)
[2] Sorlin O and Porquet M-G 2008 *Prog. Part. Nucl. Phys.* **61** 602–73
[3] Brown B A 2001 *Prog. Part. Nucl. Phys.* **47** 517–99
[4] Grawe H 2004 *Lect. Notes Phys.* **651** 33–75
[5] Caurier E *et al* 2005 *Rev. Mod. Phys.* **77** 427–88
[6] Bender M, Heenen P-H and Reinhard P-G 2003 *Rev. Mod. Phys* **75** 121–80
[7] Bender M *et al* 2004 *Phys. Rev.* C **69** 064303
[8] Bender M, Bonche P and Heenen P-H 2006 *Phys. Rev.* C **74** 024312
[9] Bender M and Heenen P-H 2008 *Phys. Rev.* C **78** 024309
[10] Rodríguez-Guzmán R, Egido J L and Robledo L M 2002 *Nucl. Phys.* A **709** 201–35
[11] Rodríguez-Guzmán R, Egido J L and Robledo L M 2004 *Phys. Rev.* C **69** 054319
[12] Delaroche J-P *et al* 2010 *Phys. Rev.* C **81** 014303
[13] Nikšić T, Vretenar D and Ring P 2006 *Phys. Rev.* C **74** 064309
[14] Nikšić T *et al* 2009 *Phys. Rev.* C **79** 034303
[15] Harakeh M *et al* (eds) 2004 *NuPECC Long Range Plan 2004: Perspectives for Nuclear Physics Research in Europe in the Coming Decade and Beyond* http://www.nupecc.org/pub/lrp03/long_rang_plan_2004.pdf
[16] Geesaman D F *et al* 2006 *Annu. Rev. Nucl. Part. Sci.* **56** 53–92
[17] Ahearne J F *et al* (eds) 2007 *Scientific Opportunities with a Rara-Isotope Facility in the United States* (Washington, DC: The National Academies Press)
[18] Gade A and Glasmacher T 2008 *Prog. Part. Nucl. Phys.* **60** 161–224
[19] Raman S, Nestor C W Jr and Tikkanen P 2001 *At. Data Nucl. Data Tables* **78** 1–128
[20] Krane K S and Steffen R M 1970 *Phys. Rev.* C **2** 724–34
[21] Cline D 1986 *Annu. Rev. Nucl. Part. Sci.* **36** 683–716
[22] Stone N J 2005 *At. Data Nucl. Data Tables* **90** 75–176
[23] Alder K and Winther A 1975 *Electromagnetic Excitation, Theory of Coulomb Excitation with Heavy Ions* (Amsterdam: North-Holland)
[24] Huus T and Zupancic C 1953 *Kgl. Danske Videnskab. Selskabs Mat.-Fys. Medd.* **28** No.1
[25] McClelland C I and Goodman C 1953 *Phys. Rev.* **91** 760–1
[26] Newton J O and Stephens F S 1958 *Phys. Rev. Lett.* **1** 63–5
[27] Stephens F S, Diamond R M and Perlman I 1959 *Phys. Rev. Lett.* **3** 435–8
[28] Winther A and de Boer J 1966 in *Coulomb Excitation* Alder K and Winther A (eds) (New York: Academic Press)
[29] Czosnyka T, Cline D and Wu C Y 1983 *Bull. Am. Phys. Soc.* **28** 745–6
[30] Hasselgren L and Cline D 1980 *Proc. Int. Conf. on Interacting Bose-Fermi Systems in Nuclei* (New York: Plenum) p 59–64
[31] Kotliński B *et al* 1990 *Nucl. Phys.* A **517** 365–85
[32] Wollersheim H J *et al* 1993 *Nucl. Phys.* A **556** 261–80
[33] Wu C Y *et al* 1996 *Nucl. Phys.* A **607** 178–234
[34] Hayes A B *et al* 2007 *Phys. Rev.* C **75** 034308
[35] de Boer J and Eichler J 1968 *Advan. Nucl. Phys.* **1** 1–65
[36] Brenn R *et al* 1977 *Z. Phys.* A **281** 219–27
[37] Motobayashi T *et al* 1995 *Phys. Lett.* B **346** 9–14
[38] Anne R *et al* 1995 *Z. Phys.* A **352** 397–401
[39] Scheit H *et al* 1996 *Phys. Rev. Lett.* **77** 3967–70
[40] Bürger A *et al* 2005 *Phys. Lett.* B **622** 29–34
[41] Glasmacher T 1998 *Ann. Rev. Nucl. Part. Sci.* **48** 1–31
[42] Winther A and Alder K 1979 *Nucl. Phys.* A **319** 518–32
[43] Cook J M, Glasmacher T and Gade A 2006 *Phys. Rev.* C **73** 024315
[44] Nolan P J and Sharpey-Schafer J F 1979 *Rep. Prog. Phys.* **42** 1–86
[45] Alexander T K and Foster J S 1979 *Advan. Nucl. Phys.* **10** 197–331
[46] Dewald A, Harissopulos S and von Brentano P 1989 *Z. Phys.* A **334** 163–75

[47] Dewald A *et al* 2003 *Phys. Rev.* C **68** 034314
[48] Grahn T *et al* 2005 *Eur. Phys. J.* A **25** s01, 441–2
[49] Grahn T *et al* 2006 *Phys. Rev. Lett.* **97** 062501
[50] Grahn T *et al* 2008 *Nucl. Phys.* A **801** 83–100
[51] Mason P J R *et al* 2010 *Phys. Lett.* B **683** 17–20
[52] Mason P J R *et al* 2010 *Phys. Rev.* C **81** 024302
[53] Starosta K *et al* 2007 *Phys. Rev. Lett.* **99** 042503
[54] Chester A *et al* 2006 *Nucl. Instrum. Methods* A **562** 230–40
[55] Dewald A *et al* 2008 *Phys. Rev.* C **78** 051302(R)
[56] Valiente-Dobón J J *et al* 2009 *Phys. Rev. Lett.* **102** 242502
[57] Ljungvall J *et al* submitted to *Phys. Rev.* C
[58] Kofoed-Hansen O and Nielsen K O 1951 *Phys. Rev.* **82** 96
[59] Kofoed-Hansen O and Nielsen K O 1951 *Kgl. Danske Videnskab. Selskabs Mat.-Fys. Medd.* **26** No.7
[60] Darquennes D *et al* 1990 *Phys. Rev.* C **42** R804–6
[61] Van Duppen P *et al* 1992 *Nucl. Instrum. Methods* B **70** 393–7
[62] Mishin V I *et al* 1993 *Nucl. Instrum. Methods* B **73** 550–60
[63] Köster U *et al* 2003 *Nucl. Instrum. Methods* B **204** 347–52
[64] Kester O *et al* 2003 *Nucl. Instrum. Methods* B **204** 20–30
[65] Schmidt P *et al* 2002 *Nucl. Phys.* A **701** 550–6
[66] Wenander F 2002 *Nucl. Phys.* A **701** 528c–536c
[67] Reiter P *et al* 2002 *Nucl. Phys.* A **701** 209c–212c
[68] Stracener D W 2003 *Nucl. Instrum. Methods* B **204** 42–7
[69] Stracener D W *et al* 2004 *Nucl. Instrum. Methods* A **521** 126–35
[70] Gross C J *et al* 2000 *Nucl. Instrum. Methods* A **450** 12–29
[71] Mittig W 1998 *J. Phys. G: Nucl. Phys.* **24** 1331–9
[72] Simpson J *et al* 2000 *Acta Phys. Hung. N. S.* **11** 159–88
[73] Bricault P 2007 *Eur. Phys. J. Special Topics* **150** 227–32
[74] Ball G C *et al* 2007 *Nucl. Phys.* A **787** 118c–125c
[75] Wiescher M, Görres J and Schatz H 1999 *J. Phys. G: Nucl. Phys.* **25** R133–61
[76] Schumaker M A *et al* 2009 *Phys. Rev.* C **80** 044325
[77] Schumaker M A *et al* 2008 *Phys. Rev.* C **78** 044321
[78] Rowe P M *et al* 1978 *J. Phys. G: Nucl. Phys.* **4** 431–43
[79] Pronko J G, Lindgren R A and Bromley D A 1970 *Nucl. Phys.* A **140** 465–80
[80] Firestone R B 2004 *Nucl. Data Sheets* **103** 269–324
[81] Brown B A *et al* 1993 *Phys. Rev.* C **48** 1456–9
[82] Thibault C *et al* 1975 *Phys. Rev.* C **12** 644–57
[83] Campi X *et al* 1975 *Nucl. Phys.* A **251** 193–205
[84] Détraz C *et al* 1979 *Phys. Rev.* C **19** 164–76
[85] Wildenthal B H and Chung W 1980 *Phys. Rev.* C **22** 2260–2
[86] Watt A *et al* 1981 *J. Phys. G: Nucl. Phys.* **7** L145–8
[87] Warburton E K, Becker J A and Brown B A 1990 *Phys. Rev.* C **41** 1147–66
[88] Iwasaki H *et al* 2001 *Phys. Lett.* B **522** 227–32
[89] Pritychenko B V *et al* 1999 *Phys. Lett.* B **461** 322–8
[90] Church J A *et al* 2005 *Phys. Rev.* C **72** 054320
[91] Chisté V *et al* 2001 *Phys. Lett.* B **514** 233–9
[92] Niedermaier O *et al* 2005 *Phys. Rev. Lett.* **94** 172501
[93] Niedermaier O 2005 PhD Thesis Univ. Heidelberg http://www.ub.uni-heidelberg.de/archiv/5647/
[94] Schwerdtfeger W *et al* 2009 *Phys. Rev. Lett.* **103** 012501
[95] Utsuno Y *et al* 1999 *Phys. Rev.* C **60** 054315
[96] Caurier E, Nowacki F and Poves A 2001 *Nucl. Phys.* A **693** 374–82
[97] Tripathi V *et al* 2008 *Phys. Rev.* C **77** 034310
[98] Takeuchi S *et al* 2009 *Phys. Rev.* C **79** 054319
[99] Azaiez F *et al* 2002 *Eur. Phys. J.* A **15** 93–7
[100] Neyens G *et al* 2005 *Phys. Rev. Lett.* **94** 022501
[101] Seidlitz M 2008 *Diploma Thesis, Univ. Cologne* unpublished
[102] Utsuno Y *et al* 2004 *Phys. Rev.* C **70** 044307
[103] Pritychenko B V *et al* 2002 *Phys. Rev.* C **66** 024325
[104] Ettenauer S *et al* 2008 *Phys. Rev.* C **78** 017302
[105] Pritychenko B V *et al* 2001 *Phys. Rev.* C **63** 011305(R)

[106] Tripathi V *et al* 2005 *Phys. Rev. Lett.* **94** 162501
[107] Tripathi V *et al* 2007 *Phys. Rev.* C **76** 021301(R)
[108] Hurst A M *et al* 2009 *Phys. Lett.* B **674** 168–71
[109] Keim M *et al* 2000 *Eur. Phys. J.* A **8** 31–40
[110] Gaudefroy L *et al* 2006 *Phys. Rev. Lett.* **97** 092501
[111] Signoracci A and Brown B A 2007 *Phys. Rev. Lett.* **99** 099201
[112] Gaudefroy L *et al* 2007 *Phys. Rev. Lett.* **99** 099202
[113] Glasmacher T *et al* 1997 *Phys. Lett.* B **395** 163–8
[114] Grévy S *et al* 2005 *Eur. Phys. J.* A **25**, s01, 111–3
[115] Bastin B *et al* 2007 *Phys. Rev. Lett.* **97** 022503
[116] Nowacki F and Poves A 2009 *Phys. Rev.* C **79** 014310
[117] Zielińska M *et al* 2009 *Phys. Rev.* C **80** 014317
[118] Lalazissis G A *et al* 1999 *Phys. Rev.* C **60** 014310
[119] Rodríguez-Guzmán R, Egido J L and Robledo L M 2002 *Phys. Rev.* C **65** 024304
[120] Gade A *et al* 2003 *Phys. Rev.* C **68** 014302
[121] Dechargé J and Gogny D 1980 *Phys. Rev.* C **21** 1568–93
[122] Berger J F, Girod M and Gogny D 1991 *Comput. Phys. Commun.* **63** 365–74
[123] Mengoni D *et al* 2010 *Nucl. Phys.* A **834** 69c–71c
[124] Dossat C *et al* 2005 *Phys. Rev.* C **72** 054315
[125] Hosmer P T *et al* 2005 *Phys. Rev. Lett.* **94** 112501
[126] Broda R *et al* 1995 *Phys. Rev. Lett.* **74** 868–71
[127] Guénaut C *et al* 2007 *Phys. Rev.* C **75** 044303
[128] Rahaman S *et al* 2007 *Eur. Phys. J* A **34** 5–9
[129] Sorlin O *et al* 2002 *Phys. Rev. Lett.* **88** 092501
[130] Langanke K *et al* 2003 *Phys. Rev.* C **67** 044314
[131] Bree N *et al* 2008 *Phys. Rev.* C **78** 047301
[132] Otsuka T *et al* 2005 *Phys. Rev. Lett.* **95** 232502
[133] Perru O *et al* 2006 *Phys. Rev. Lett.* **96** 232501
[134] Robinson R L, McGowan F K and Stelson P H 1964 *Phys. Rev.* **134** B567–74
[135] Franchoo S *et al* 1998 *Phys. Rev. Lett.* **81** 3100–3
[136] Franchoo S *et al* 2001 *Phys. Rev.* C **64** 054308
[137] Stefanescu I *et al* 2008 *Phys. Rev. Lett.* **100** 112502
[138] Oros-Peusquens A M and Mantica P F 2000 *Nucl. Phys.* A **669** 81–100
[139] Flanagan K T *et al* 2009 *Phys. Rev. Lett.* **103** 142501
[140] Stefanescu I *et al* 2007 *Phys. Rev. Lett.* **98** 122701
[141] Van Roosbroeck J *et al* 2004 *Phys. Rev. Lett.* **92** 112501
[142] Weissman L *et al* 2002 *Phys. Rev.* C **65** 024315
[143] Thomas J C *et al* 2006 *Phys. Rev.* C **74** 054309
[144] Van de Walle J *et al* 2007 *Phys. Rev. Lett.* **99** 142501
[145] Van de Walle J *et al* 2009 *Phys. Rev.* C **79** 014309
[146] Kenn O *et al* 2001 *Phys. Rev.* C **65** 034308
[147] Leenhardt S *et al* 2002 *Eur. Phys. J.* A **14** 1–5
[148] Bouquerel E *et al* 2007 *Eur. Phys. J.* ST **150** 277–80
[149] Padilla-Rodal E *et al* 2005 *Phys. Rev. Lett.* **94** 122501
[150] Koo W K and Tassie L J 1981 *J. Phys. G: Nucl. Phys.* **7** L63–5
[151] McAninch J E *et al* 1995 *Nucl. Instrum. Methods* B **99** 541–5
[152] Lecomte R *et al* 1982 *Phys. Rev.* C **25** 2812–4
[153] Nazarewicz W *et al* 1985 *Nucl. Phys.* A **435** 397–447
[154] Petrovici A, Schmid K W and Faessler A 2000 *Nucl. Phys.* A **665** 333–50
[155] Yamagami M, Matsunayagi K and Matsuo M 2001 *Nucl. Phys.* A **693** 579–602
[156] Girod M *et al* 2009 *Phys. Lett.* B **676** 39–43
[157] Sarriguren P 2009 *Phys. Rev.* C **79** 044315
[158] Chandler C *et al* 1997 *Phys. Rev.* C **56** R2924–8
[159] Becker F *et al* 1999 *Eur. Phys. J.* A **4** 103–5
[160] Bouchez E *et al* 2003 *Phys. Rev. Lett.* **90** 082502
[161] Clément E *et al* 2007 *Phys. Rev.* C **75** 054313
[162] Görgen A *et al* 2005 *Eur. Phys. J.* A **26** 153–7
[163] Gade A *et al* 2005 *Phys. Rev. Lett.* **95** 022502
[164] Fischer S M *et al* 2000 *Phys. Rev. Lett.* **84** 4064–7
[165] Clément E *et al* 2008 *Nucl. Instrum. Methods* A **587** 292–9
[166] Hurst A *et al* 2007 *Phys. Rev. Lett.* **98** 072501

[167] Heese J *et al* 1986 *Z. Phys.* A **325** 45–53
[168] Ljungvall J 2008 *Phys. Rev. Lett.* **100** 102502
[169] Otsuka T *et al* 2001 *Phys. Rev. Lett.* **87** 082502
[170] Talmi I 1971 *Nucl. Phys.* A **172** 1–24
[171] Banu A *et al* 2005 *Phys. Rev.* C **72** 061305(R)
[172] Vaman C *et al* 2007 *Phys. Rev. Lett.* **99** 162501
[173] Cederkäll J *et al* 2007 *Phys. Rev. Lett.* **98** 172501
[174] Ekström A *et al* 2008 *Phys. Rev. Lett.* **101** 012502
[175] Ekström A *et al* 2010 *Eur. Phys. J.* A in press
[176] Doornenbal P *et al* 2008 *Phys. Rev.* C **78** 031303(R)
[177] Kumar R *et al* 2010 *Phys. Rev.* C **81** 024306
[178] Ansari A 2005 *Phys. Lett.* B **623** 37–42
[179] Ekström A *et al* 2009 *Phys. Rev.* C **80** 054302
[180] Köster U *et al* 2008 *Nucl. Instrum. Methods* B **266** 4229–39
[181] Boelaert N *et al* 2007 *Phys. Rev.* C **75** 054311
[182] Chen B *et al* 1995 *Phys. Lett.* B **355** 37–44
[183] Mach H, Gill R L and Moszynski M 1989 *Nucl. Instrum. Methods* A **280** 49–72
[184] Smith A G *et al* 2002 *J. Phys. G: Nucl. Phys.* **28** 2307–16
[185] Smith A G *et al* 1994 *Phys. Rev. Lett.* **77** 1711–14
[186] Radford D *et al* 2002 *Phys. Rev. Lett.* **88** 222501
[187] Barton C J *et al* 2003 *Phys. Lett.* B **551** 269–76
[188] Radford D *et al* 2005 *Nucl. Phys.* A **752** 264c–272c
[189] Radford D *et al* 2005 *Eur. Phys. J.* A **25** s01, 383–7
[190] Varner R L *et al* 2005 *Eur. Phys. J.* A **25** s01, 391–4
[191] Kröll Th *et al* 2005 *Proc. Int. Symp. on Exotic Nuclear Systems* ed Gácsi Z *et al* (AIP Conf. Proc. vol 802) p 283–6
[192] Kröll Th *et al* 2007 *Eur. Phys. J.* ST **150** 127–9
[193] Kröll Th *et al* 2008 *Proc. Frontiers in Nuclear Structure, Astrophysics, and Reactions* ed Demetriou P *et al* (AIP Conf. Proc. vol 1012) p 84–8
[194] Jakob G *et al* 2002 *Phys. Rev.* C **65** 024316
[195] Terasaki J *et al* 2002 *Phys. Rev.* C **66** 054313
[196] Ansari A and Ring P 2006 *Phys. Rev.* C **74** 054313
[197] Severyukhin A P, Voronov V V and Nguyen Van Giai 2008 *Phys. Rev.* C **77** 024322
[198] Coraggio L *et al* 2002 *Phys. Rev.* C **65** 051306(R)
[199] Sarkar S and Sarkar M S 2004 *Eur. Phys. J.* A **21** 61–6
[200] Kartamyshev M P *et al* 2007 *Phys. Rev.* C **76** 024313
[201] Shimizu N *et al* 2004 *Phys. Rev.* C **70** 054313
[202] Grodzins L 1962 *Phys. Lett.* **2** 88–91
[203] Wood J L *et al* 1992 *Phys. Rep.* **215** 101–201
[204] Bonn J *et al* 1972 *Phys. Lett.* B **38** 308–11
[205] Julin R, Helariutta K and Muikku M 2001 *J. Phys. G: Nucl. Phys.* **27** R109–39
[206] Van Duppen P *et al* 1984 *Phys. Rev. Lett.* **52** 1974–77
[207] Andreyev A N *et al* 2000 *Nature (London)* **405** 430–3
[208] De Coster C, Decroix B and Heyde K 2000 *Phys. Rev.* C **61** 067306
[209] May F R, Pashkevich V V and Frauendorf S 1977 *Phys. Lett.* B **68** 113–6
[210] Petts A *et al* 2009 *Proc. Capture Gamma-Ray Spectroscopy and Related Topics* ed Blazhev A *et al* (AIP Conf. Proc. vol 1090) p 414–8
[211] Rud N *et al* 1973 *Phys. Rev. Lett.* **31** 1421–23
[212] Proetel D, Diamond R M and Stephens F S 1974 *Phys. Lett.* B **48** 102–4
[213] Grahn T *et al* 2009 *Phys. Rev.* C **80** 014324
[214] Scheck M *et al* 2010 *Phys. Rev.* C **81** 014310
[215] Riisager K 2008 *Proc. Frontiers in Nuclear Structure, Astrophysics, and Reactions* ed Demetriou P *et al* (AIP Conf. Proc. vol 1012) p 106–10
[216] Gales S 2008 *Proc. Frontiers in Nuclear Structure, Astrophysics, and Reactions* ed Demetriou P *et al* (AIP Conf. Proc. vol 1012) p 94–105
[217] Blumenfeld Y *et al* 2009 *Nuclear Physics News* **19** 22–7
[218] http://www.frib.msu.edu/
[219] Simpson J 2006 *J. Phys: Conference Series* **41** 72–80
[220] Lee I-Y 2009 *Proc. XXXI Workshop on Nuclear Physics in Brazil* ed Guimaraes V *et al* (AIP Conf. Proc. vol 1139) p 23-8
[221] Eberth J and Simpson J 2008 *Prog. Part. Nucl. Phys.* **60** 283–337